

AD-A092 320

RAYTHEON CO WALTHAM MA RESEARCH DIV
POWER FET CONTACT TECHNOLOGY.(U)
SEP 80 R MOZZI, Y TAJIMA

F/G 9/1

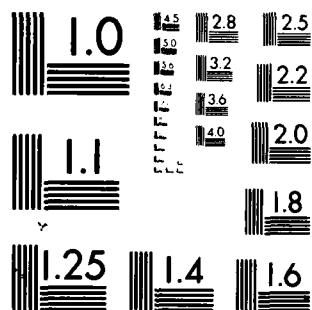
UNCLASSIFIED 5-2796

N00014-78-C-0622

NL

106/1
2094 500

END
DATE
FILMED
DTIC



MICROCOPY RESOLUTION TEST CHART
NATIONAL BUREAU OF STANDARDS 1963-A

LEVEL II

(12)

AD A092320

N00014-78-C-0622

POWER FET CONTACT TECHNOLOGY

Raytheon Company
Research Division
28 Seyon Street
Waltham, Massachusetts 02254

DTIC
ELECTE
DEC 02 1980
S D
E

September 1980

TECHNICAL REPORT

Final Report for Period September 1, 1978 to July 31, 1980

Approved for public release; distribution unlimited.

Reproduction, in whole or in part, is permitted for any purpose of the U. S. Government.

Office of Naval Research
Department of the Navy
Arlington, Virginia 22217

DDC FILE COPY

SECURITY CLASSIFICATION OF THIS PAGE (When Data Entered)

REPORT DOCUMENTATION PAGE		READ INSTRUCTIONS BEFORE COMPLETING FORM
1. REPORT NUMBER	2. GOVT ACCESSION NO.	3. RECIPIENT'S CATALOG NUMBER
	AD-A0912 320	
4. TITLE (and Subtitle)	5. TYPE OF REPORT & PERIOD COVERED	
POWER FET CONTACT TECHNOLOGY.	Final Technical Report 9/1/78-7/31/80	
6. AUTHOR(s)	7. PERFORMING ORG. REPORT NUMBER	
R. Mozzi, Y. Tajima	S-2796	
	8. CONTRACT OR GRANT NUMBER(s)	
	N00014-78-C-0622	
9. PERFORMING ORGANIZATION NAME AND ADDRESS	10. PROGRAM ELEMENT, PROJECT, TASK AREA & WORK UNIT NUMBERS	
Raytheon Research Division 28 Seyon Street Waltham, Massachusetts 02254	PE62762N RF.62.581.001 NR 251-034	
11. CONTROLLING OFFICE NAME AND ADDRESS	12. REPORT DATE	
ONR, Department of the Navy 800 N. Quincy Street Arlington, Virginia 22217	September 1980	
14. MONITORING AGENCY NAME & ADDRESS (if different from Controlling Office)	15. SECURITY CLASS. (of this report)	
(12) 49	Unclassified	
	15a. DECLASSIFICATION DOWNGRADING SCHEDULE	

16. DISTRIBUTION STATEMENT (of this Report)

Approved for public release; distribution unlimited.

17. DISTRIBUTION STATEMENT (of the abstract entered in Block 20, if different from Report)

18. SUPPLEMENTARY NOTES

ONR Scientific Officer: Telephone (203) 696-4218

19. KEY WORDS (Continue on reverse side if necessary and identify by block number)

Pulsed electron beam annealed implants, vapor phase epitaxy, unalloyed ohmic contact layers, n-type GaAs, power FETs.

20. ABSTRACT (Continue on reverse side if necessary and identify by block number)

Unalloyed TiPtAu ohmic contacts were formed on n-type GaAs by preparing surfaces having over 10^{18} carriers/cm² prior to metal deposition. Two methods were used, vapor phase epilayer growth and pulse electron beam annealed (PEBA) selenium implants. The former method yielded specific contact resistivities (8×10^{-6}) Ω cm² and was successfully applied on power FET devices. Much lower resistivities, (3×10^{-7}) Ω cm², were obtained by PEBA implants but difficulties associated with preserving channel layers through the PEBA exposure have precluded their application in a device configuration.

DD FORM 1 JAN 73 1473

EDITION OF 1 NOV 65 IS OBSOLETE

* < 01 =

2983

SECURITY CLASSIFICATION OF THIS PAGE (When Data Entered)

(c) approx 2000 ohm sq cm

ACKNOWLEDGEMENTS

The authors are indebted to several co-workers for their contributions to this study. We especially want to thank William Labossier who prepared the epilayer depositions, Frank Piekarski who performed the ion implants and differential sheet resistivity and Hall measurements, Ann Kirkpatrick, Joan Jampsa, Angelo Amato, and Dorothy Bell for device fabrication and mounting, and Susan Trulli who made most of the contact resistance and dc electrical checks. We also thank Dr. Otto Guentert for the excellent SEM photographs.

Our thanks are extended to Dr. Robert Kaplan of Quantronix Corporation for the laser exposures, Dr. Anton Greenwald of Spire Corporation for the pulsed electron beam exposures and Dr. Charles Evans of Charles Evans Associates for the SIMS analyses.

We are also grateful to Mr. Max Yoder of ONR for his suggestions and to the Office of Naval Research for their support of this program.

Accession For	
NTIS GRA&I	<input checked="" type="checkbox"/>
DDC TAB	<input type="checkbox"/>
Unannounced	<input type="checkbox"/>
Justification	
By	
Distribution/	
Availability Codes	
Dist	Availability and/or special
A	

TABLE OF CONTENTS

<u>SECTION</u>	<u>PAGE</u>
I INTRODUCTION	1
II LASER-ANNEALED SAMPLES	4
III PULSE ELECTRON BEAM ANNEAL (PEBA) STUDIES	10
A. Summary of Experiments and Results	10
1. Exposure Set #1	10
2. Exposure Set #2	14
3. Exposure Set #3	14
4. Exposure Set #4	15
B. Experimental Procedures	15
1. PEBA Exposures	15
2. Measurement Procedures	16
C. PEBA Results	26
1. PEBA-Annealed Implant Profiles	29
2. Profiles with Reduced Implant Dose and PEBA Fluence	35
IV FURNACE ANNEALED CO-IMPLANTS OF SELENIUM AND SILICON	49
V HIGHLY DOPED GROWN EPILAYER SURFACES	51
A. Carrier Profiles	51
B. Contact Resistances and Thermal Stability	54
C. Power FETs with Unalloyed Contacts	56
VI SUMMARY	59
REFERENCES	61

LIST OF ILLUSTRATIONS

<u>FIGURE</u>		<u>PAGE</u>
1	SEM photographs of laser-irradiated stripes on GaAs sample 40576B.	6
2	PEBA apparatus electron beam diode voltage and current measurements and analytically determined energy distribution	11
3	Normalized depth-dose profile (calculated) in GaAs using the electron energy spectrum shown in Fig. 2 with a 60° angle of incidence	12
4	Temperature versus time at different depths in GaAs for the beam parameters given in Figs. 2 and 3.	13
5	(a) Cloverleaf mesa used for differential Hall mobility and sheet resistance measurements. (b) Exploded view of circular ion milling sample holder showing (1) sapphire mask, (2) GaAs sample and platform, and (3) one of three positioning screws.	18
6	A semi-empirical graph of resistivity versus carrier concentration for grown n-type epilayers.	20
7	Heating cycle for alloying contacts.	22
8	Carrier profiles of a PEBA Se implant without post-PEBA heating (a) and after a simulated alloying heat treatment (b).	23
9	(a) Sample 1-41614-3: optical photograph at 40X after PEBA. (b) SEM photograph at 20 KX after PEBA and HCl dip.	28
10	Nonuniform V/I measured across 1.5 cm of sample 2-41639-6.	30
11	X-ray reflection topograph of sample 2-41639-6 after PEBA, showing nonuniform strain distribution	30
12	Carrier and mobility profile of 2-41639-1, implanted with 5×10^{15} Se/cm ² at 120 keV with 0.67 J/cm ² PEBA.	32
13	Carrier and mobility profile of 2-41639-2 implanted with 5×10^{15} Se/cm ² at 120 keV with 0.67 J/cm ² PEBA after deposition and removal of a CVD Si ₃ N ₄ film.	32
14	Carrier and mobility profiles of 2-41639-4 (X) and 2-41639-5 (O) implanted with 5×10^{15} Se/cm ² at both 120 and 320 keV, with 0.67 J/cm ² PEBA.	32
15	SIMS and carrier profiles before and after PEBA	33

LIST OF ILLUSTRATIONS (Concluded)

<u>FIGURE</u>		<u>PAGE</u>
16	Carrier profiles for PEBA Se implants of $5 \times 10^{14}/\text{cm}^2$ at both 120 and 320 keV (a) plus additional Si implants of $5 \times 10^{13}/\text{cm}^2$ (b) and $2 \times 10^{14}/\text{cm}^2$ (c) at both 50 and 130 keV.	36
17	Sheet resistances of a PEBA Se implant as a function of PEBA fluence.	37
18	C-V measured carrier profiles after PEBA with fluences of (b) $0.59 \text{ J}/\text{cm}^2$ and c) $0.84 \text{ J}/\text{cm}^2$ compared with a) the original epilayer profile.	39
19	(a) Photograph of boundary region (640 \times) showing masked region (left) and annealed implant region (right); (b) Dektak trace across boundary with scales indicated.	44
20	SEM photo of the transition region on 3-7A90-1 between the masked portion at left and the PEBA implant at right after removal of the SiO_x and gallium residues.	45
21	a) Optical photograph at 64X of 4-7B118-1 after a localized implant in the device pattern and an unmasked PEBA; b) Two alignment squares opened and implanted with the source-drain pattern.	46
22	SEM photos of 3-7A91-6.	48
23	Calculated and measured profiles for furnace annealed Se-Si implants.	50
24	Carrier and mobility profile of a grown epilayer having an n^{++} surface.	52
25	Carrier concentration profiles for increased silane flow times.	53
26	Electrical profile of epilayer 7B166B and SIMS profile of epilayer 7B129A.	55
27	SEM photo of power FET and cross-sectional schematic of an individual cell.	57
28	Power FET output power versus input power, wafer 82625, device #2.	58

LIST OF TABLES

<u>TABLE</u>		<u>PAGE</u>
I	Diameters of Concentric Circles Formed by Laser Pulses on GaAs	5
II	Summary of Laser Anneal Experiments	7
III	Results of Preliminary PEBA Implants	27

SECTION I

INTRODUCTION

Degradation of ohmic contact layers on n-type gallium arsenide is known to be a common cause of device failure, particularly at the elevated temperatures and high current densities encountered, for example, in power field effect transistors (FETs).¹⁻⁷ Contacts are usually formed by depositing thin-film composites containing gold, germanium, and nickel which are subsequently alloyed above the Au-GaAs eutectic temperature, for example at 460°C for less than 1 minute. Indiffusion of germanium facilitated by nickel forms a highly doped n^{++} layer at the metal-GaAs interface; the contact is ohmic, primarily because of tunneling through the metal-semiconductor barrier.⁸ No highly stable interface is formed, however, and interdiffusion of the various atomic species persists under thermal and electrical stresses imposed by device operation. The very mechanisms that enable these contacts to be formed contribute to their gradual degradation.

Reliability limitations of Ni, Au, Ge-type contacts have motivated a search for methods of forming much more stable contacts. In addition to being thermally and electrically stable, the contacts must satisfy the following conditions.

1. The contacts must be ohmic, with the lowest possible resistance. This implies that the carrier concentration in the GaAs at the interface should be as high as possible above $10^{19}/\text{cm}^3$, and should extend at least as deep as the space charge depletion layer at zero bias.⁹
2. The metallization should be formed reproducibly with good adhesion, morphology, and mechanical strength and be easily bondable to external circuitry.

The approach we have chosen has been to prepare an n^{++} GaAs surface with over 10^{19} carriers/ cm^3 prior to metal deposition, so that dopant indiffusion from the metallization is not required, and then to use a refractory metal system, which is less likely to interact with GaAs during operation of the completed device. The metal system used was gold over platinum over titanium on GaAs. It adheres well to GaAs, no interdiffusion occurs at least up to 350°C,¹⁰ and the gold can

be plated to form a sturdy, easily bondable contact. This composite is readily and reproducibly prepared by sequential electron-beam evaporation of titanium and platinum and resistive-heated evaporated gold. It also forms good Schottky-barrier contacts on n-type GaAs and may therefore be used for FET gates as well, thus yielding some simplification in FET fabrication.

Various ways of preparing n^{++} GaAs surfaces that were tried included:

1. Vapor-phase epilayer growth of a silicon-doped n^{++} layer over the usual silicon-doped n-type active FET layer.
2. Co-implants of silicon and selenium into silicon-doped n-type epilayers. furnace-annealed under Si_3N_4 caps.
3. Laser-annealed selenium implants into silicon-doped n-type epilayers.
4. Electron-beam-annealed implants of selenium and co-implants of silicon and selenium combined in silicon doped n-type epilayers.

The bulk of our effort was expended on those two approaches that looked most immediately promising, namely, vapor-phase-grown n^{++} layers and electron-beam-annealed selenium implants. We have grown n^{++} layers whose carrier concentration peaks at over 10^{19} carriers/cm³ in a very thin (about 100 Å) layer at the immediate surface. Contact resistivities of TiPtAu layers on these samples have been as low as $8 \times 10^{-6} \Omega\text{cm}^2$, and high-quality power FETs have been made with unalloyed TiPtAu contacts, even for samples with contact resistivities as high as $10^{-4} \Omega\text{cm}^2$.

By far the most impressive contacts were made on pulse electron beam annealed (PEBA) selenium-implanted layers. Contact resistivities in the low $10^{-7} \Omega\text{cm}^2$ range were consistently obtained and remained at this level even after extended thermal stress tests at 250°C. However, unimplanted n-type layers suffer a severe decrease in carrier concentration during PEBA exposure and some way must be found to preserve the n layer if PEBA implants are to be localized in the contact

regions of a device pattern. We tried to save the n layer in two ways, first by using the minimum possible PEBA fluence to anneal the localized implants, with the hope of minimizing damage to the n layer, and next by selectively shielding the unimplanted n-type regions with thick photoresist or deposited SiO_x . Although both approaches showed some promise in experiments on uniformly grown or implanted layers, neither was successful in a device configuration. The experiments performed and the results obtained will be discussed.

Laser anneals were also attempted at the beginning of this study. Their effectiveness in achieving high carrier concentrations was comparable to PEBA anneals, but the resultant GaAs surface appearance was poor and we chose to restrict our radiation anneal studies to the PEBA type.

Furnace-annealed co-implants of silicon and selenium failed to yield peak concentrations as high as $10^{19}/\text{cm}^3$ and this method was not pursued beyond a first unsuccessful trial.

SECTION II

LASER-ANNEALED SAMPLES

Several authors have published studies of at least two different approaches to forming ohmic contacts on GaAs with the help of lasers. In the first approach, the usual procedure using a AuGe composite is followed, except that furnace alloying of the metal-GaAs interface is replaced by exposure to short (tens of nanoseconds) or long (about 1 ms) laser pulses.¹¹⁻¹⁴ In the second approach, a highly doped n^{++} layer is formed by ion implantation, and laser activation of the implant is used instead of a furnace anneal.^{15,16} Harrison and Williams¹⁷ reported simultaneous implant anneal and metallization alloying using CO_2 laser radiation incident through the backside of the wafer.

Our studies consisted of only one set of nine samples, pulse-annealed at Quantronics Corporation using a modified Model 603 laser scribe. The incident beam parameters were:

Wavelength: 0.53 μm by second harmonic generation of a Nd-YAG laser with no 1.06 μm beam on samples.

Pulse Rate: 2 kHz

Pulse Width: 70 nsec

Pulse Power: About 0.12 watts - variable using crossed polarizers

Beam Profile: Gaussian with a 124 μm diameter at 1/e of peak intensity

The sample was located on a table open to air which moved at an adjustable constant speed v_y back and forth in one direction and stepped at a settable distance Δx in a perpendicular direction at the end of each pass.

In a preliminary test run on a GaAs blank, $v_y = 8$ in./sec, $\Delta x = 5$ mils, visual inspection at low magnification revealed that each pulse produced concentric circles of diameter d_1 and d_2 . The inner area showed small specks and

the area bounded by the two circles resembled a resolidified melt. Table I shows the approximate values of d_1 and d_2 as a function of pulse power.

TABLE I
DIAMETERS OF CONCENTRIC CIRCLES
FORMED BY LASER PULSES ON GaAs

<u>Energy (Joules/cm²)</u>	<u>d₁ (μm)</u>	<u>d₂ (μm)</u>
0.5	42	91
0.4	28	63
0.3	0	42
0.2	0	0

The inner circle was interpreted as the boundary within which the Gaussian-shaped pulse raised the temperature above the vaporization point and the outer circle as the boundary within which the temperature exceeded the melting point. SEM photos of another piece scanned under various conditions are shown in Fig. 1. In this experiment we were looking for conditions which formed an overlap of spots where melting had apparently occurred with little vaporization. The range 0.25 to 0.4 J/cm² was selected for exposures on implanted GaAs samples.

Implants were 5×10^{15} Se⁺/cm² at 120 keV at either 25° or 300°C into epitaxial buffer layers over 3.8 μm thick, grown on chromium-doped semi-insulating substrates obtained from Monsanto. The results of laser anneals on these samples are shown in Table II.* The sample surfaces were bare during both implant and anneal and the anneals were done in an unenclosed system open to the room ambient. Sheet resistivities were measured with a four-point probe and room

* Samples in this report will be identified by an epilayer growth run number which has internal-Raytheon significance as a reference to our data filing system. A prefix followed by a dash refers to a set of samples radiation annealed on the same day. Prefixes only appear on PEBA samples. A suffix following a dash indicates a subsection cleaved from a larger wafer on which the epilayer was grown. For example, 1-41614-2 designates section #2 cleaved from epilayer wafer 41614 and annealed with the first set of PEBA runs.

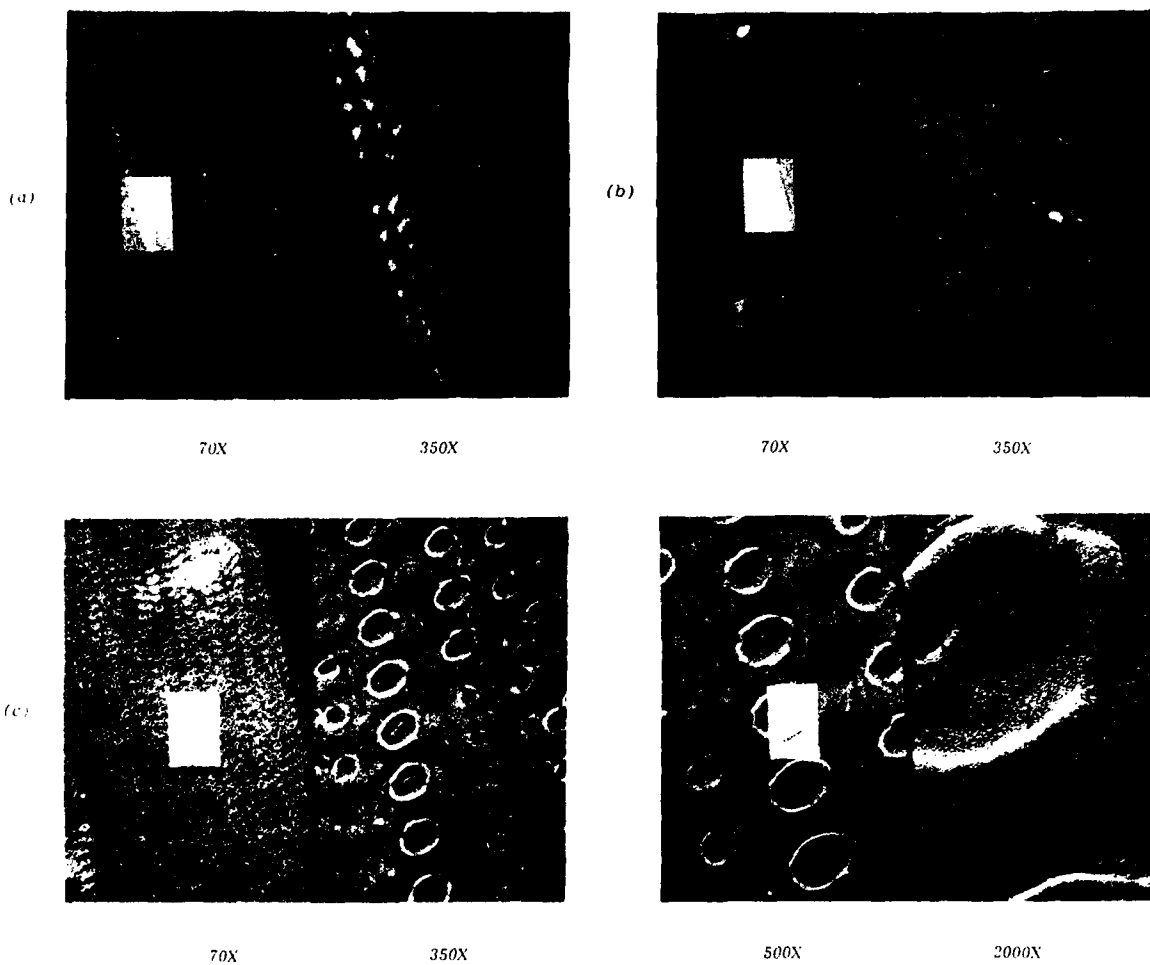


Figure 1. SEM photographs of laser-irradiated stripes on GaAs sample 40576B. The lightened rectangles in the lefthand sectors indicate the area shown enlarged on the righthand side. Scan parameters for these photographs are tabulated.

SCAN PARAMETERS			
	$P(J/cm^2)$	$V_s(in/sec)$	$X(mils)$
(a)	0.2	1	0.5
(b)	0.3	2	1.0
(c)	0.4	3	1.5

TABLE II
SUMMARY OF LASER ANNEAL EXPERIMENTS

Sample	Implant Temperature (°C)	Laser Fluence (J/cm^2) v_y (in/sec) Δx (mils)	ρ (Ω/\square) 4 Pt. Probe	\bar{N}_s (cm^{-2}) Hall	$\bar{\mu}_H$ ($\text{cm}^2/\text{v sec}$)
41614-12	25	0.25	1250
		1.0			
		0.5			
82470-2	300	0.25	1250
		1.0			
		0.5			
41614-6	25	0.35	85	135	1.3×10^{14} 350
		3.0			
		1.5			
41614-5	300	0.40	80	138	1.3×10^{14} 350
		3.0			
		1.5			

temperature Hall measurements of the sheet resistance, average carrier surface concentration N_S and mobility μ were made on two of the samples using a van der Pauw clover leaf formed on the sample. Discrepancies between the four-point probe and clover leaf sheet resistances are due to the heating used to alloy the clover leaf contacts and will be discussed further in the PEBA studies section. Surface damage was visible on all of the samples in the form of overlapping rings at 0.25 J/cm^2 progressing to overlapping craters about $1 \text{ }\mu\text{m}$ deep at 0.4 J/cm^2 . Each sample also showed a dense distribution of white spots, which were removable in an HCl dip. The sheet resistivities suggest a fluence above 0.25, and less than 0.4 J/cm^2 is required for best activation, note from Fig. 1 that there is severe surface damage for fluences $\geq 0.3 \text{ J/cm}^2$.

An unimplanted wafer (72673) of the type typically used for device fabrication was cleaved in half and one half was laser annealed to evaluate how FET channel regions might be affected during laser anneals of device wafers having localized high-dose implants in the source drain contact regions. (The unused half was saved for an electron beam exposure.) Prior to anneal, capacitance versus voltage (C,V) measurements of this sample using 16-mil diameter Au-on-Al Schottky-barrier diodes indicated a flat profile with $7.5 \times 10^{16} \text{ carriers/cm}^3$ to a depth of $0.45 \text{ }\mu\text{m}$, then dropping rapidly to about $5 \times 10^{15}/\text{cm}^3$ at $0.55 \text{ }\mu\text{m}$. After anneal, CV measurements showed an average of only $7.7 \times 10^{15} \text{ carriers/cm}^3$ to a depth of about $0.38 \text{ }\mu\text{m}$ (which was the zero bias depletion depth), then decreasing to join the unannealed profile at about $0.65 \text{ }\mu\text{m}$. Evidently some means of protecting channel regions would be necessary if laser-annealed contacts were to be used on FET device wafers.

To compare the depth of carrier removal relative to the laser beam penetration we may use the optical constants for GaAs at room temperature given by Seraphin and Bennett.¹⁸ Writing the refractive index

$$n = u + iv$$

and interpolating the data for $\eta = 0.53 \text{ }\mu\text{m}$, we find

$$u \approx 3.97, v \approx 0.313$$

$$\alpha = 4\pi v/\lambda = 7.3 \mu\text{m}^{-1}$$

The reflectivity R is

$$R = \frac{(u_2 - 1)^2 + v^2}{(u_2 + 1)^2 + v^2} = .36$$

and the transmitted fraction at depth X , $T(X)$ is

$$T(X) = (1-R)e^{-\alpha X} = 0.64 e^{-7.3 X(\mu\text{m})}$$

which indicates that 90 percent of the unreflected intensity is absorbed within $0.31 \mu\text{m}$ of the surface. These optical constants are only applicable at the first instant of exposure, since they may vary greatly during exposure with the rising temperature and distortion of the sample.

The sheet resistivities obtained after laser anneals were higher than the lowest values measured for PEBA anneals of samples that were otherwise identical. Differential Hall and sheet resistance measurements were not made, so the peak carrier concentrations were not determined and no attempt was made to form unalloyed contacts on these samples, since the PEBA procedure looked much more promising.

SECTION III

PULSE ELECTRON BEAM ANNEAL (PEBA) STUDIES

A. SUMMARY OF EXPERIMENTS AND RESULTS

Electron-beam exposures were done over a period of about one year at Spire Corporation under the direction of Dr. Anton Greenwald, and using equipment and procedures described by Greenwald and co-workers.¹⁹ The equipment and service were rented for a total of four days, one each in the months of November 1978, February 1979, October 1979, and February 1980. Although the samples exposed on each day formed a self-contained experiment, it seems advisable to report the results of each day as a separate unit, in view of the fact that the equipment and procedures were under continuing improvement during the year, so that there may be differences in conditions and calibrations from one day to another.

Except for a few samples run with the first exposure set, all of our PEBA exposures had an electron energy distribution similar to the one shown in Fig. 2. The mean energy of this distribution is 20 keV, and the pulse duration was about 100 ns. Figure 3 shows a Monte Carlo calculation of the depth distribution of deposited energy (J/gram) per unit fluence (J/cm^2) for the energy distribution in Fig. 2 with an angle of incidence of 60° . (The experimentally determined angle of incidence is about 45° , but this should not significantly change the curve). Figure 4 shows the temperature-time curves at various depths calculated for the energy deposition in Fig. 3. (Figures 2, 3, and 4 were provided by Dr. Greenwald).

The purpose and result of each day's experiments may be summarized as follows.

1. Exposure Set #1

Five selenium-implanted samples were exposed to determine roughly what electron beam fluence, energy and implant temperature would yield the lowest sheet resistance and hence be likely to produce the highest surface carrier concentration. A fluence of about $0.7 \text{ J}/\text{cm}^2$ with electrons having a mean energy

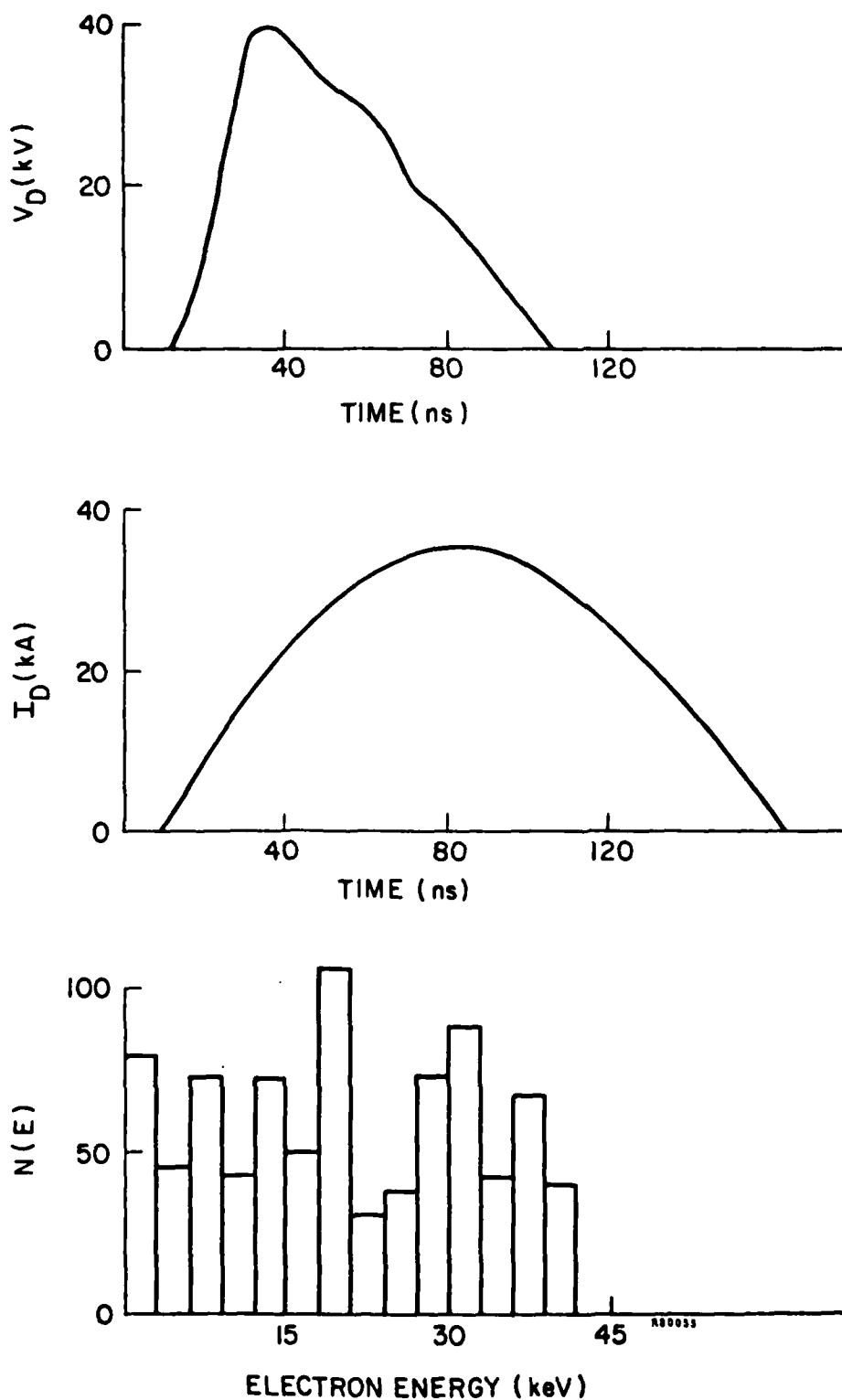


Figure 2. PEBA apparatus electron beam diode voltage and current measurements and analytically determined energy distribution.

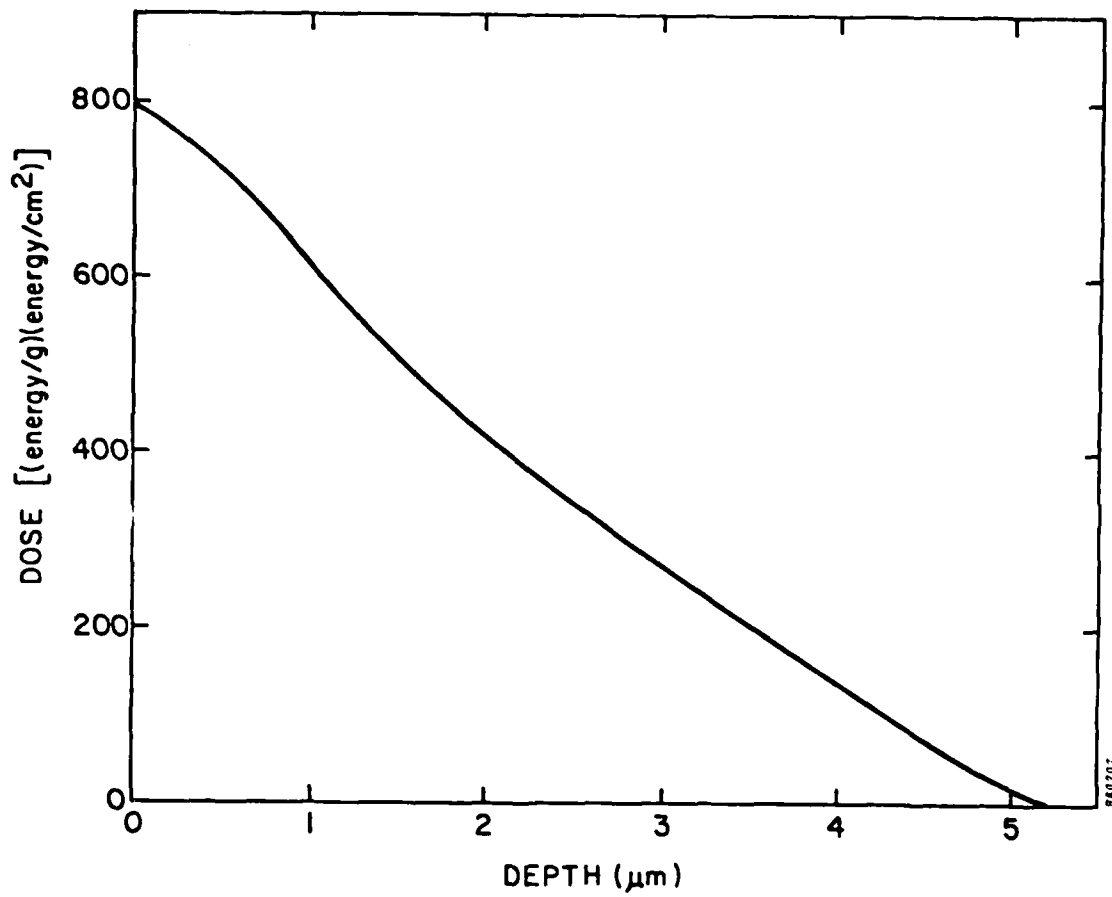


Figure 3. Normalized depth-dose profile (calculated) in GaAs using the electron energy spectrum shown in Fig. 2 with a 60° angle of incidence.

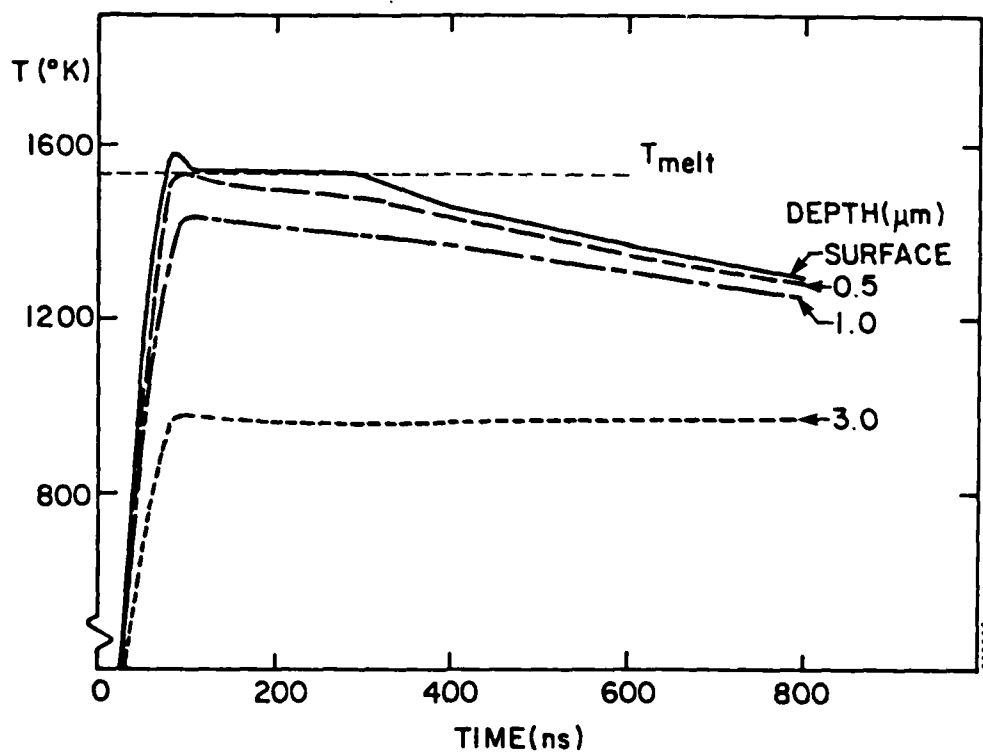


Figure 4. Temperature versus time at different depths in GaAs for the beam parameters given in Figs. 2 and 3.

of 20 keV incident on a sample implanted at room temperature looked best and the surface appearance, after an HCl dip to remove residual surface Ga, was excellent. However, the carrier concentration of an unimplanted 0.6 μm thick n-type epilayer was eliminated by a fluence of 0.67 J/cm^2 , indicating the need for some protection of channel regions in FET material exposed to PEBA.

2. Exposure Set #2

Guided by the results of Set #1, room temperature selenium implants were PEBA annealed at 0.67 J/cm^2 and samples were prepared for differential carrier profile and mobility determinations.

Unalloyed TiPtAu was also deposited in a ladder test pattern for contact resistance measurements. The results indicated carrier concentrations exceeding $10^{19}/\text{cm}^3$ and contact resistivities as low as $3 \times 10^{-7} \Omega\text{cm}^2$. Other samples in this set were exposed to evaluate the suitability of SiO_x and AZ1350J photoresist as protective coatings for channel-type layers during PEBA. Minimal changes in carrier profiles resulted from a fluence of 0.7 J/cm^2 on samples coated with 0.7 μm SiO_x or 2 μm of AZ1350J. However, similar coating thicknesses over the channel regions of a power-FET pattern were ineffective, indicating that a patterned structure behaved differently from either fully implanted and uncoated or fully coated and unimplanted layers.

3. Exposure Set #3

Three questions were addressed in this series: (1) What is the nature of the boundary between an implanted, uncovered surface and an unimplanted, covered surface after PEBA exposure? (2) Do co-implants of selenium and silicon offer an advantage? (3) What effect does post-PEBA heating have on PEBA implants?

We found that, for the case of a sample on which a large, bare, implanted area adjoined a large covered area, the boundary was marked by a severe distortion of the GaAs surface, making it unlikely that a patterned mask could

be used in an FET geometry. Se-Si co-implants yielded carrier concentrations exceeding $10^{19}/\text{cm}^3$ for lower implant doses than were obtained with selenium alone, and thermal annealing at up to 250°C in hydrogen produced an increase in the sheet resistance of bare implanted layers but the resistance of unalloyed contacts either decreased or was unchanged.

4. Exposure Set #4

The final exposures were designed to see whether an intermediate fluence could be found which was high enough to form ohmic contacts in implanted regions but low enough to retain sufficient carrier concentration in an n-type epilayer to form an FET channel. A fluence of about $0.58 \text{ J}/\text{cm}^2$ showed some promise, but attempts to make devices were unsuccessful.

In the discussions that follow, a prefix 1, 2, 3, or 4 will be attached to each sample number to designate which exposure set it belongs to.

B. EXPERIMENTAL PROCEDURES

1. PEBA Exposures

The samples used were taken from a supply of our in-house-grown epilayers on purchased semi-insulating substrates. Most samples were n-type layers on buffer layers of the type typically used for power-FET fabrication, except that no samples with n^{++} layers were used, since one goal of our studies was to replace grown n^{++} layers covering the entire surface with PEBA localized implants. Thick buffer layers without an n-type surface layer were used in some of the earlier experiments. We felt that it was important to use device-type material in order to be sure that our results would be relevant to device fabrication and to avoid the vagaries associated with chromium-doped semi-insulating material at least to the depths to which the implants and anneals would be affected. All samples were at least $1 \times 1 \text{ cm}^2$ to reduce the importance of edge effects during the PEBA exposure. They were prepared for exposure by a thorough cleaning, including organic solvents, buffered HF, and finally a rinse in deionized water.

Samples were mounted in the PEBA vacuum system on a turntable which allowed six samples to be rotated into the incident beam individually with a single vacuum pumpdown. The turntable contained six holders, each of which consisted of a circular graphite plate on an aluminum supporting disk. A Chomerics Company conductive black grease was used to stick the sample backs to the graphite plate except on the exposures in Set #1. One of the six sample positions was left unloaded to provide a location for trial exposures. Trial exposures were made with each loading to "precondition" the system or, by inserting a calorimeter in the beam, to measure and adjust the fluence. The vacuum was $10^{-5} - 5 \times 10^{-4}$ torr at the initiation of each pulse and the voltage and current waveforms of each pulse were recorded on a curve tracer photograph. It was estimated that less than 10^{12} carbon atoms/cm² may have been deposited from the filament with each pulse.

After the samples were removed from the system, grease was removed with trichloroethylene, acetone, methanol, and water, and samples were examined with an optical microscope.

2. Measurement Procedures

After cleaning, microscope examination, and an HCl dip and water rinse to remove gallium residues, the following procedures were used in the preparation and measurement of samples.

a. Sheet resistance

Four-point probe measurements were made on an A. M. Fell Resistivity Model A test rig. The probes had a 0.005 in. radius and a 1 mm spacing between tips. Fixed currents of 0.01, 0.10, and 1.0 mA were used, and the voltages were measured on a Boonton Model 95A dc voltmeter.

b. Capacitance-voltage carrier profiles

Schottky-barrier diodes were made by depositing gold over aluminum on GaAs in a pattern in which a 16 mil diameter AlAu dot was isolated from an

AlAu field by a concentric $35 \times 35 \text{ mil}^2$ square of GaAs which was uncovered except for the central dot. C-V measurements were made with one probe on a dot and the other on the field. For profiles too deep to be measured with a single dot, other dots were used which were deposited on previously etched steps of known depth. This is a procedure routinely used in our laboratory to characterize grown epilayers. C-V profiles were measured, converted to carrier-depth profiles and plotted by an automated profiler.

c. Differential sheet resistance and Hall mobility profiles

Carrier concentration and mobility profiles were measured on a van der Pauw clover-leaf pattern, shown in Fig. 5a, which consists of a mesa rising above a background of GaAs etched down into the semi-insulating substrate. Pads for contacts at the four extremities were an alloyed NiAuGe composite film. Carrier and mobility profiles were obtained from sheet resistance and Hall mobility measurements alternating with layer removal. Original attempts using 1:1:100 H_2O_2 , H_2SO_4 , H_2O at 1°C gave erratic results and we resorted to charge-neutralized 0.5 keV, 0.7 mA/cm^2 argon ions in a Veeco Microetch ion-milling system. The region outside the dashed circle in Fig. 5a was shielded from the argon beam by the sapphire mask in a holder shown schematically in Fig. 5b. The sapphire, which was chosen for its low milling rate, rests a few mils above the GaAs, and the sample was stuck to its aluminum pedestal with Dow Corning 340 heat transfer paste.

The total depth etched was monitored by a step height determination on a small piece of the GaAs slice mounted near the sapphire aperture and partially masked by photoresist. The measured etch rate was 750 \AA/min .

At first, the sample and platform were removed from the ion miller after every etch step and measurements were made at room temperature in a fixture having four probes and fitting between the poles of an electromagnet. Hall measurements were made with a field of 4000 gauss. Later the fixture was modified to allow wires bonded to the pads to pass through holes in the platform and out through vacuum feedthroughs in the ion-miller so that sheet resistance

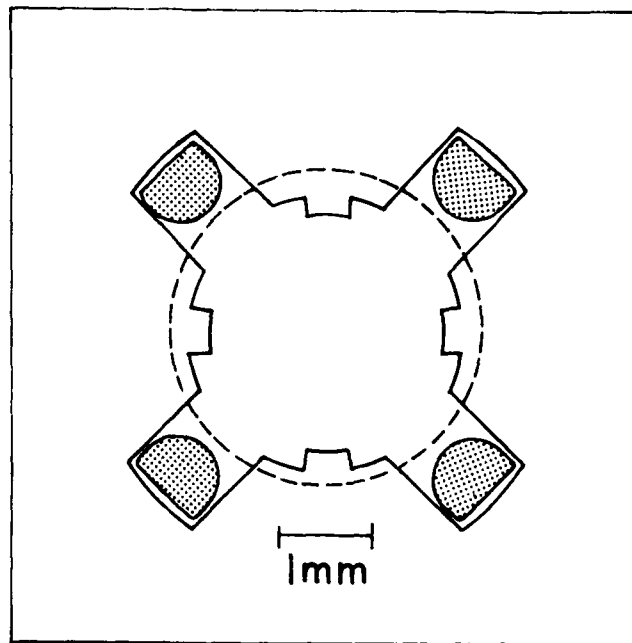


Figure 5(a). Cloverleaf mesa used for differential Hall mobility and sheet resistance measurements. Regions outside the dashed circle were masked from the ion milling beam.

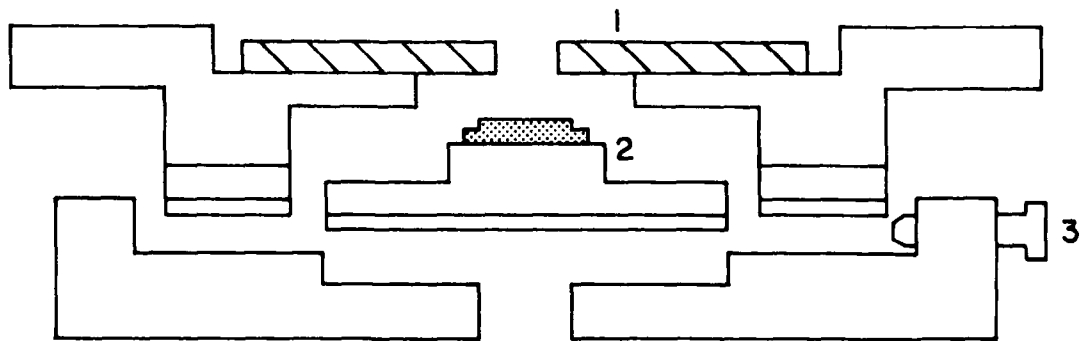


Figure 5(b). Exploded view of circular ion milling sample holder showing (1) sapphire mask, (2) GaAs sample and platform, and (3) one of three positioning screws.

measurements could be made in situ. Sheet resistance measurements were then usually made at 125 Å intervals and Hall measurements at 1250 Å intervals. This change saved considerable time that had previously been spent waiting for the vacuum system to pump down.

The average carrier concentration $n(X)$ and mobility $\mu(X)$ of a layer extending in depth from X to $X + \Delta X$ were obtained from Hall mobility μ and sheet resistance R measurements made before and after removal of a layer ΔX thick. Using subscripts i and j to refer respectively to measurements made before and after, we have:

$$\mu(X) = (\mu_i R_j - \mu_j R_i) / (R_j - R_i)$$

$$n(X) = r(R_j - R_i) / \mu(X) e \Delta X R_i R_j$$

where $e = 1.6 \times 10^{19}$ coulombs is the electronic charge and r is the ratio of Hall to drift mobility, which we have assumed to be approximately equal to 1.

In the case of grown epilayers we found that it was possible to construct a semi-empirical graph, shown in Fig. 6, of the sheet resistivity ρ (ohms cm) versus n which was consistent with the $n(X)$ and $\mu(X)$ measurements of typical samples. This made it possible to omit the Hall measurements and instead very rapidly measure $\rho(X)$ from in-situ measurements of R_i, R_j :

$$\rho(X) = R_i R_j \Delta X / (R_j - R_i)$$

and then read $n(X)$ from the ρ versus n graph.

The use of ion milling raises the question of how the radiation damage induced by the milling argon atoms might affect the measurements. Our feeling was that based on Range statistics for 0.5 keV argon ions, a layer no thicker than about 50 Å might become insulating as a result of the argon beam, and since this layer would be present after every milling step it should have little effect on differential measurements except for the first etch step. This

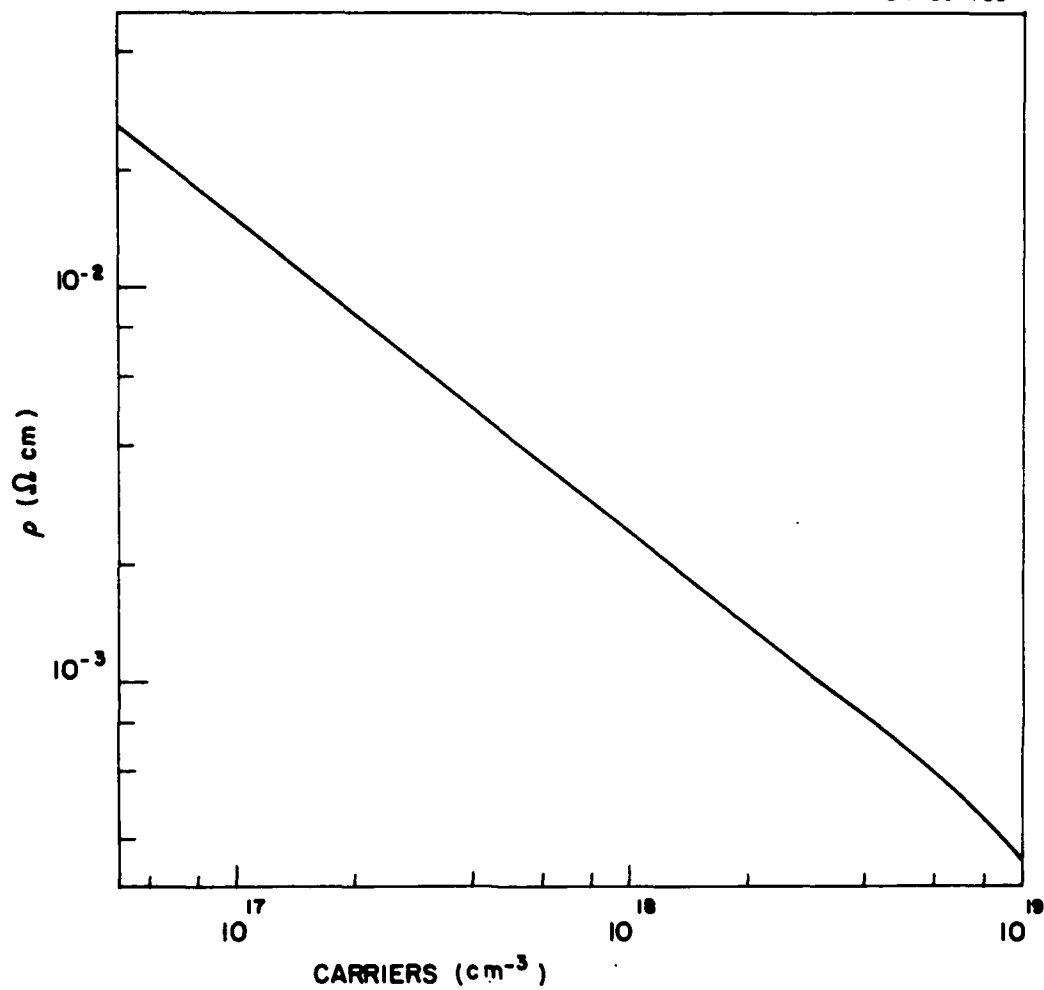


Figure 6. A semi-empirical graph of resistivity versus carrier concentration for grown n-type epilayers.

step would have an effective removal depth equal to the depth milled off ΔX plus some additional damaged depth ϵ . This has the approximate effect of removing the depth increment from ΔX to $\Delta X + \epsilon$ from the profile and transferring the carriers in this increment into the first ΔX interval, yielding an artificially high $n(x)$ in this interval. This error is unimportant for our PEBA profiles but may be significant for the shallow surface peaks we found on grown n^{++} epilayers. There may have been some more subtle effect due, for example to damage-induced strain gradients. We did not investigate this possibility.

Of greater significance is the fact that the carrier and mobility profile present after PEBA is altered by the heat treatment involved in forming the NiAuGe contact pads which we formed on the Hall samples. The alloying step which is done in a hydrogen ambient consists of the temperature versus time schedule shown in Fig. 7. To see the effect of the heating used for alloying we split the lower half of sample 3-7A25A in half and formed a clover leaf pattern with TiPtAu contact pads on each piece. One piece was then heated with the same schedule and in the same furnace used to alloy NiAuGe contacts and differential profiles were measured on each piece.

At the beginning, sample 3-7A25A was $1.7 \times 2.3 \text{ cm}^2$ with an n-type epilayer $1.3 \times 10^{17} \text{ carriers/cm}^3$, $0.2 \text{ }\mu\text{m}$ thick and a $2.0 \text{ }\mu\text{m}$ thick buffer layer. It was implanted at room temperature with $5 \times 10^{15} \text{ Se/cm}^2$ at both 120 and 320 keV and PEBA annealed with 20 keV electrons at 0.71 J/cm^2 . The carrier profiles of the unheated and heated clover-leaf pattern are shown in Fig. 8. The sheet resistances prior to the first milling were 49 and 85 ohms/sq. for the unheated and heated pieces respectively and the mobilities averaged over the first $1250 \text{ }\text{\AA}$ were $124 \text{ cm}^2/\text{V-sec}$ for the unheated sample and $297 \text{ cm}^2/\text{V-sec}$ for the heated sample. (The peak carrier concentration of the unheated sample, about $8.5 \times 10^{19}/\text{cm}^3$, is higher than any we have seen reported for GaAs.)

Comparison of the profiles in Fig. 8 shows that a significant reduction in carrier concentration accompanies the simulated alloying step. (Similar effects have been reported by Pianetta and co-workers.²⁰) In retrospect, it is now clear that many of our Hall samples would not have required alloyed contact pads, and if unalloyed contacts had been used the profiles would have been more representative of the situation immediately after PEBA. A difference in the sheet resistance measured on the four-point probe setup before forming the van der Pauw

P8N-80-657

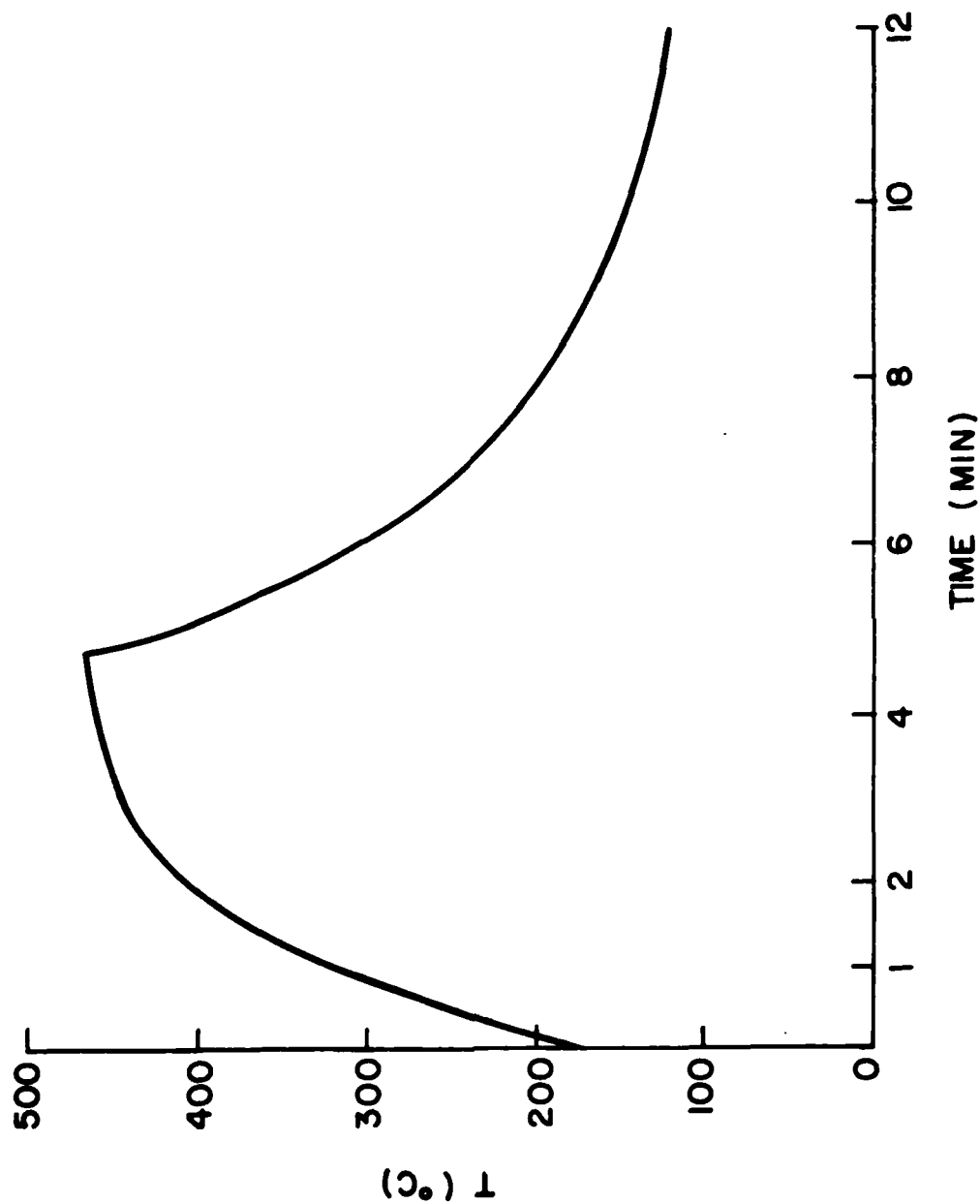


Figure 7. Heating cycle for alloying contacts.

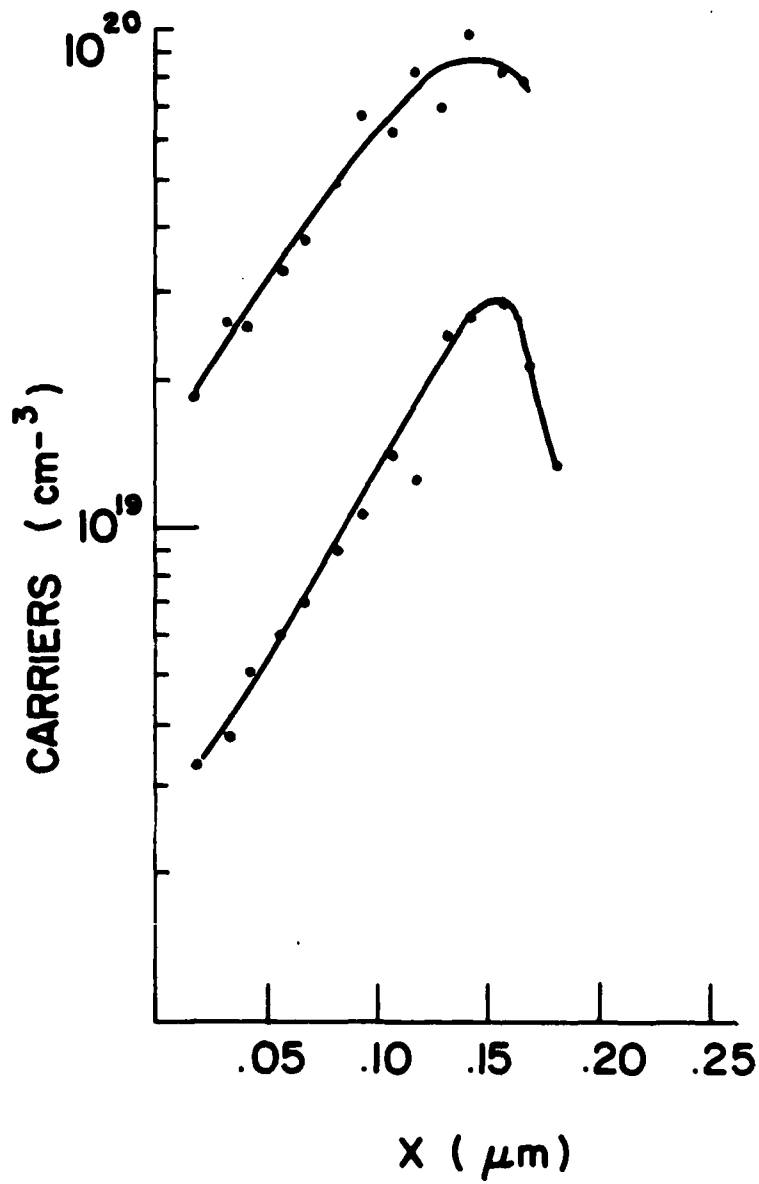


Figure 8. Carrier profiles of a PEBA Se implant without post-PEBA heating (a) and after a simulated alloying heat treatment (b).

pattern and then later on the completed pattern using the alloyed contacts was observed on the first samples measured. But the profiles subsequently measured had less than 10^{19} carriers/cm² at the immediate surface and it was questionable whether ohmic contacts would be formed without etching to near the carrier concentration peak. We therefore decided to use alloyed contacts on all the Hall samples rather than introduce another variable into the measurements. The reader should therefore bear in mind that in this report the carrier profiles which were obtained by differential sheet resistance and mobility measurements represent the results of PEBA plus the additional alloying heat cycle and that the carrier concentrations without the alloying cycle would generally be higher for PEBA samples.

d. Specific contact resistance measurements

Specific contact resistances of unalloyed TiPtAu contacts on PEBA surfaces were made using the transmission line contacts (TLC)²¹⁻²⁴ method. The contact pattern was photolithographically defined in Shipley AZ1350 photoresist and immediately before metal deposition a few hundred Å were chemically etched and the sample was rinsed in 5 percent NH₄OH to remove any surface oxide. The surface was then coated by electron beam vapor deposition of either 500 or 1000 Å titanium followed by either 500 or 1000 Å platinum and 3000 Å of evaporated gold.

Metallization not over the contacts was removed by dissolving the photoresist. The TLC patterns were then masked by photoresist and the surrounding GaAs was ion milled into the high-resistivity buffer layer. The completed TLC mesas consisted of five 67×254 -μm (L × Z) TiPtAu pads separated by gaps of $l = 5.5, 10.8, 15.7, \text{ and } 21.0$ μm. These final dimensions were measured by microscope on the completed patterns.

The specific contact resistance was determined using the equation²¹

$$R = (R_{\square}/Z)[1 + 2L_t \coth (L/L_t)]$$

where R is the sheet resistance, L is the contact length, Z is the contact width, l is the spacing between contacts, and L_t is the transfer length given by

$$L_t^2 = r_c / R_{\square},$$

where r_c is the specific contact resistance ($\Omega \text{ cm}^2$). Independent current and voltage probes were used and measurements were made with a current of 10 mA. Several patterns were measured and a least-squares fit of the data for each pattern was used to determine R_{\square} and r_c . For these patterns the contact resistance is only about 20 percent of the total even for the narrowest 5.5- μm gap and is therefore difficult to measure accurately. Fits with correlation coefficients $r < 0.9995$, where

$$r = \frac{N \sum R_i l_i - \sum R_i \sum l_i}{[\sum l_i^2 - (\sum l_i)^2]^{1/2} [N \sum R_i^2 - (\sum R_i)^2]^{1/2}}$$

and where $N = 4$ is the number of data points, were therefore rejected in order to use only the most consistent results.

e. Secondary ion mass spectroscopy

SIMS measurements were made by Charles Evans and Associates using a CAMECA IMS-3f and a cesium ion beam. Normalization of the submitted samples relative to one another was made on the basis of the amount of sputtered and mass separated arsenic collected in a Faraday cup and the ^{69}Ga intensity was traced during each run as a stability check. The final normalization was based on two submitted standards:

Standard #1 - $5 \times 10^{14} \text{ SiH}^+/\text{cm}^2$ at 240 keV implanted at Raytheon into a Metals Research undoped GaAs semi-insulating substrate.

Standard #2 - $5 \times 10^{15} \text{ Se}/\text{cm}^2$ at 120 keV + $5 \times 10^{15} \text{ Se}/\text{cm}^2$ at 320 keV implanted at Raytheon into another substrate of the same type.

The normalization constant was determined from the ratio of the implanted dose to the integrated SIMS profile.

The depth scale was established by a Dektak surface profile measurement of the depth of the sputtered depression.

f. Scanning electron microscopy

SEM photographs were taken on an AMR-1200 scanning electron microscope.

C. PEBA RESULTS

The first PEBA run was designed to provide a rough comparison with laser annealing and to indicate whether elevated temperature implants would be required and what PEBA conditions would be appropriate. From the results summarized in Table III it was clear that room temperature implants annealed with a fluence of about 0.67 J/cm^2 were most promising. All of the implanted samples were $1 \times 1 \text{ cm}^2$ sections cleaved from the same original epilayer wafer #41614 which had a $10 \text{ }\mu\text{m}$ thick buffer layer ($< 10^{14} \text{ carriers/cm}^3$) grown on a chromium-doped semi-insulating substrate. The implants were $5 \times 10^{15} \text{ Se/cm}^2$ at 120 keV. Two sheet resistance measurements are given for some samples to show the result of the alloying heat treatment, one measured with a four-point probe prior to forming the van der Pauw clover leaf and one on the clover leaf with alloyed contact pads. The average sheet carrier concentration and Hall mobility are from a single measurement without layer removals.

The visible results of PEBA annealing of GaAs are shown in Fig. 9a, which is an optical microscope picture of sample 1-41614-3. This sample was annealed with 0.85 J/cm^2 which is too high and the damage is therefore exaggerated relative to what is observed for $\lesssim 0.7 \text{ J/cm}^2$. The spotted white background is typical although the spot density varies considerably over any sample. The rings were not generally present at lower fluences, nor were the vertical and horizontal stripes, each of which envelopes a central slip line or microcrack, easily visible in a microscope, along the crystallographic $[011]$ and $[0\bar{1}\bar{1}]$ cleavage directions normal to the (100) surface. After an HCl dip the background regions are featureless even on this overly irradiated sample.

Figure 9b is a SEM photograph of one of the slip lines at 20 KX magnification after an HCl dip; the absence of any detail in the background shows the

TABLE III

RESULTS OF PRELIMINARY PEBA IMPLANTS

Sample	Implant Temperature (°C)	PEBA Mean Electron Energy (kev)	PEBA Fluence (J/cm ²)	4 Pt Probe ρ (Ω/\square)	Hall \bar{N}_s (cm ⁻²)	$\frac{\bar{\mu}H}{2}$ (cm ² /v sec)
1-41614-1	300	30 < \bar{E} < 50	0.42	> 10 ⁵
1-41614-2	300	30 < \bar{E} < 50	0.63	90	1.2 × 10 ¹⁴	190
1-41614-3	300	30 < \bar{E} < 50	0.85	> 10 ⁵
1-41614-4	300	20	0.67	> 10 ⁵
1-41614-8	25	20	0.67	42	79	430

Figure 9(a). SEM photograph at 10X after PEBA.

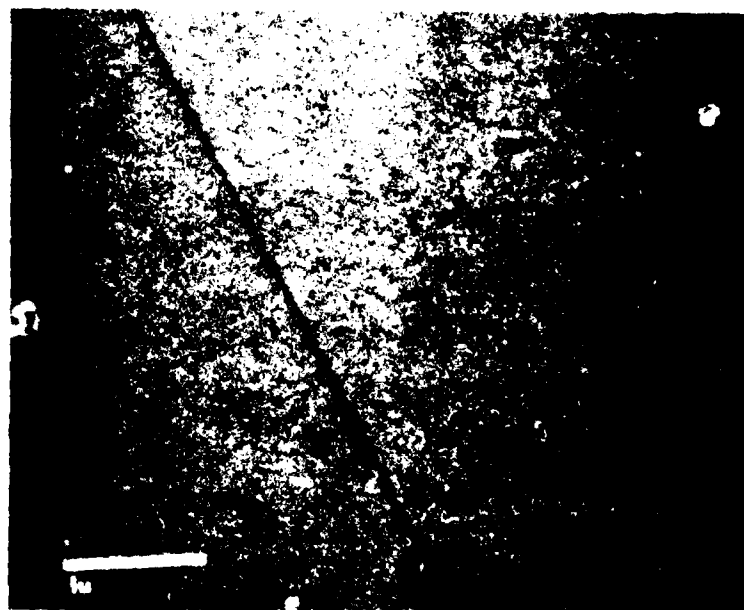


Figure 9(b). SEM photograph at 20 KX after PEBA and HCl dip.

high quality of the GaAs surface, particularly in comparison with laser-annealed samples. On the other hand, the nonuniform patterns of residual gallium which we typically observed suggests that there must be inhomogeneities either in the impacting electron beam or in the way in which regions of the sample react to the beam. Figure 10 shows an example of a nonuniform V/I measured by a four-point probe at equal intervals from one end to another of a $1.2 \times 1.5 \text{ cm}^2$ sample, 2-41639-6, which was implanted at room temperature with $5 \times 10^{15} \text{ Se/cm}^2$ at 120 keV plus $5 \times 10^{15} \text{ Se/cm}^2$ at 320 keV and PEBA annealed at 0.71 J/cm^2 . Figure 11, an X-ray reflection topograph of 2-41639-5, which was implanted and annealed in the same manner as 2-41639-6, shows evidence of a nonuniform strain distribution. Unfortunately, no topograph was made prior to PEBA so we cannot be sure that the strain was not present beforehand; however, we consider this to be only a remote possibility, since this pattern does not resemble any of the many topographs we have taken in the past. As will be shown later, any nonuniformity in the surface topography of a GaAs sample during PEBA presents more serious problems.

An unimplanted epilayer wafer 1-72673-2 was also irradiated with these preliminary exposures to determine what might happen to FET channel-type layers during PEBA. The original epilayer had a silicon-doped n-type carrier concentration of $7.2 \times 10^{16}/\text{cm}^3$ to a depth of $0.6 \text{ }\mu\text{m}$ over a $2 \text{ }\mu\text{m}$ buffer layer. After PEBA no residual carrier concentration was measurable by C-V profiling. As in the case of laser annealing, degradation of channel-type layers poses a problem for device applications, which will have to be solved if PEBA anneals are to be used to form unalloyed ohmic contacts.

1. PEBA-Annealed Implant Profiles

Carrier concentration and mobility profiles were measured on several PEBA samples during the course of this program. After the first trial exposures, which yielded low sheet resistances (1-41614-8), we wanted to determine whether and at what depth the concentration might exceed $10^{19}/\text{cm}^3$, which we felt would be necessary to form unalloyed contacts. In subsequent experiments we hoped to assess what minimum implant doses and PEBA fluences would be adequate in order to minimize the possible disadvantages of excessive amounts of inactive

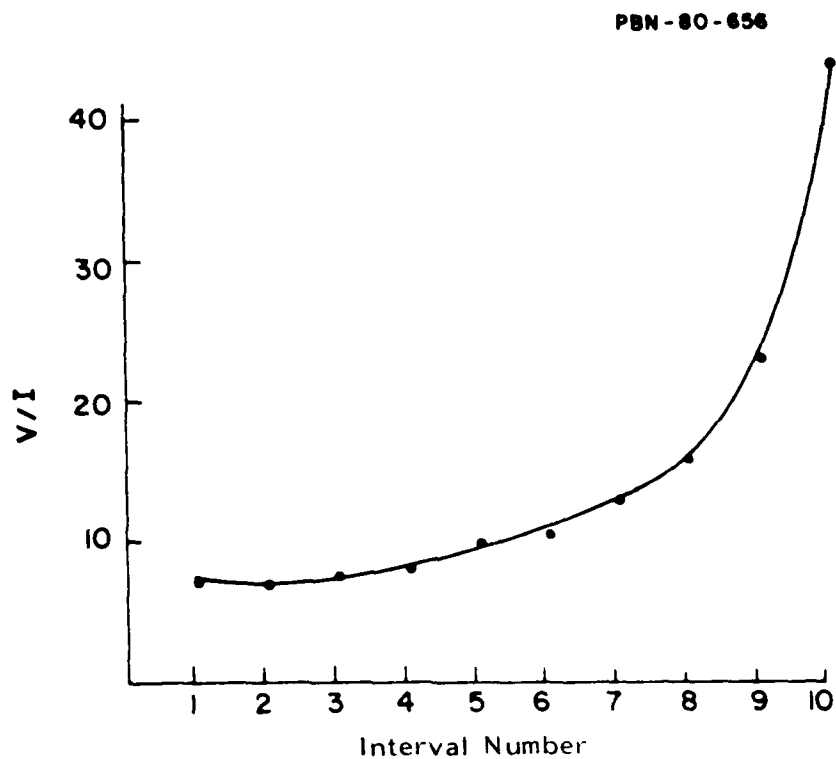


Figure 10. Nonuniform V/I measured across 1.5 cm of sample 2-41639-6.



PBN-80-1027

Figure 11. X ray reflection topograph of sample 2-41639-6 after PEBA, showing nonuniform strain distribution.

dopants, and of implant and PEBA damage. We also measured the profile change introduced by deposition of a CVD Si_3N_4 film after PEBA, since we considered using Si_3N_4 to provide passivation for devices, and we evaluated co-implants of silicon and selenium.

Figures 12-14 show the carrier and mobility profiles measured on 2-41639-1, 2, 4, 5. These were $1.2 \times 1.5 \text{ cm}^2$ sections of a $3 \times 3.6 \text{ cm}^2$ epilayer wafer with a $0.33 \text{ }\mu\text{m}$ thick silicon-doped epilayer surface having $9.2 \times 10^{16} \text{ carriers/cm}^3$ on a $4 \text{ }\mu\text{m}$ buffer layer. All six pieces of the wafer were PEBA annealed at 0.67 J/cm^2 . Numbers 2 through 6 were implanted at room temperature with $5 \times 10^{15} \text{ Se/cm}^2$ at 120 keV. An additional implant of $5 \times 10^{15} \text{ Se/cm}^2$ was added to numbers 4, 5, and 6.

The tabulated projected range and standard deviation of 120 KeV Se^+ in GaAs are $0.044 \text{ }\mu\text{m}$ and $0.021 \text{ }\mu\text{m}$ respectively.²⁴ Figure 12 therefore shows that diffusion occurred during PEBA and shifted the peak of the carrier distribution to about $0.12 \text{ }\mu\text{m}$. The sheet resistance rose abruptly to over $12 \text{ K } \Omega/\square$ after removing about $0.2 \text{ }\mu\text{m}$, suggesting that the original $0.33 \text{ }\mu\text{m}$, $9.2 \times 10^{16}/\text{cm}^3$ epilayer had been altered. Most important, however, is the fact that the maximum carrier concentration exceeds $10^{19}/\text{cm}^3$. Samples 4 and 5 also have concentrations above $10^{19}/\text{cm}^3$. The additional $5 \times 10^{15} \text{ Se/cm}^2$ at 320 KeV on these samples appear to provide the advantage of a higher carrier concentration at the immediate surface. In view of the nonuniformity of sample 6 from this wafer shown in Fig. 10, however, the general validity of this result would require further confirmation.

Figure 15 shows the result of a SIMS analysis of sample 3-7A25B-3. Sample 7A25B was a $1.7 \times 2.2 \text{ cm}^2$ epiwafer with a $2 \text{ }\mu\text{m}$ thick buffer layer and a silicon-doped, $0.22 \text{ }\mu\text{m}$ thick, $1.3 \times 10^{17} \text{ carriers/cm}^3$ surface. It was implanted with $5 \times 10^{15} \text{ Se/cm}^2$ at both 120 and 320 keV and PEBA annealed at 0.71 J/cm^2 . Following an HCl dip, 30 second H_2O_2 - NH_4OH etch, and 5 percent NH_4OH rinse, 1000, 1000, 3000 \AA TiPtAu was deposited as part of a thermal stability experiment on pieces 1 and 2, which will be discussed later. The sample was cleaved into $5 \times 5 \text{ mm}^2$ pieces and on piece 3 the gold and platinum were ion milled, the titanium removed by a 15 second dip in 2 percent HF, and the sample submitted for SIMS analysis along with all of the SIMS samples discussed in this report.

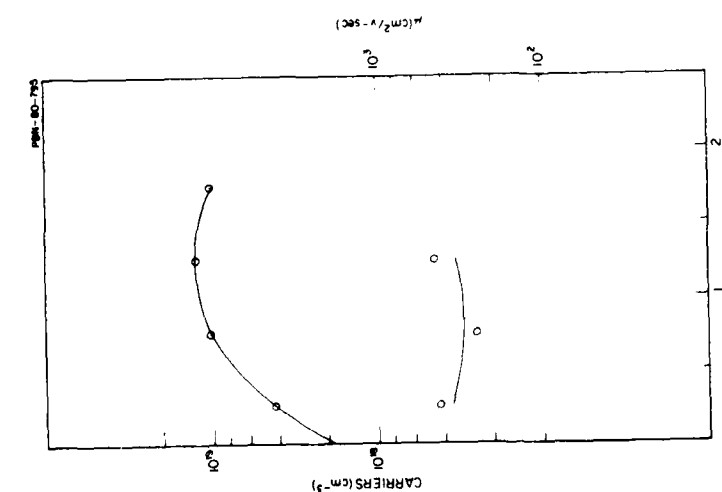


Fig. 12 Carrier and mobility profiles of 2-41639-1, implanted with 5×10^{15} Se/cm² at 120 keV with 0.67 J/cm² PEBA.

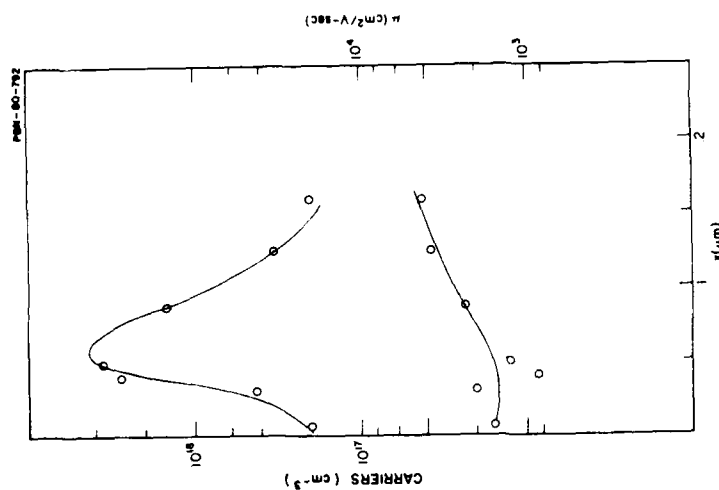


Fig. 13 Carrier and mobility profiles of 2-41639-2 implanted with 5×10^{15} Se/cm² at 120 keV with 0.67 J/cm² PEBA after deposition and removal of a CVD Si₃N₄ film.

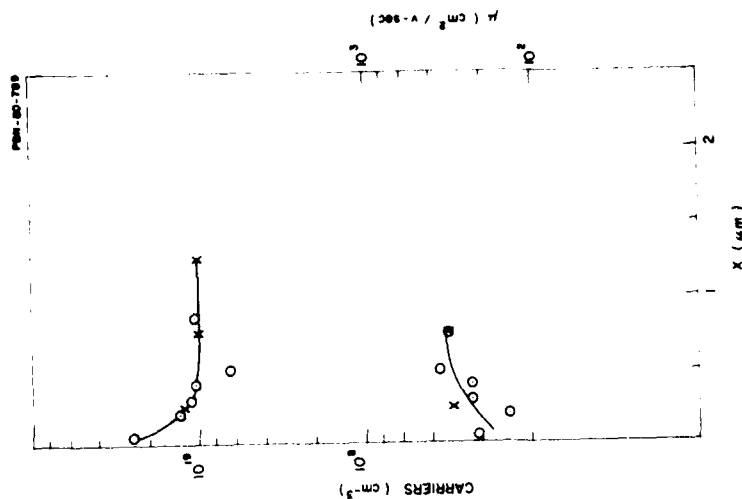


Fig. 14 Carrier and mobility profiles of 2-41639-4 (X) and 2-41639-5 (O) implanted with 5×10^{15} Se/cm² at both 120 and 320 keV, with 0.67 J/cm² PEBA.

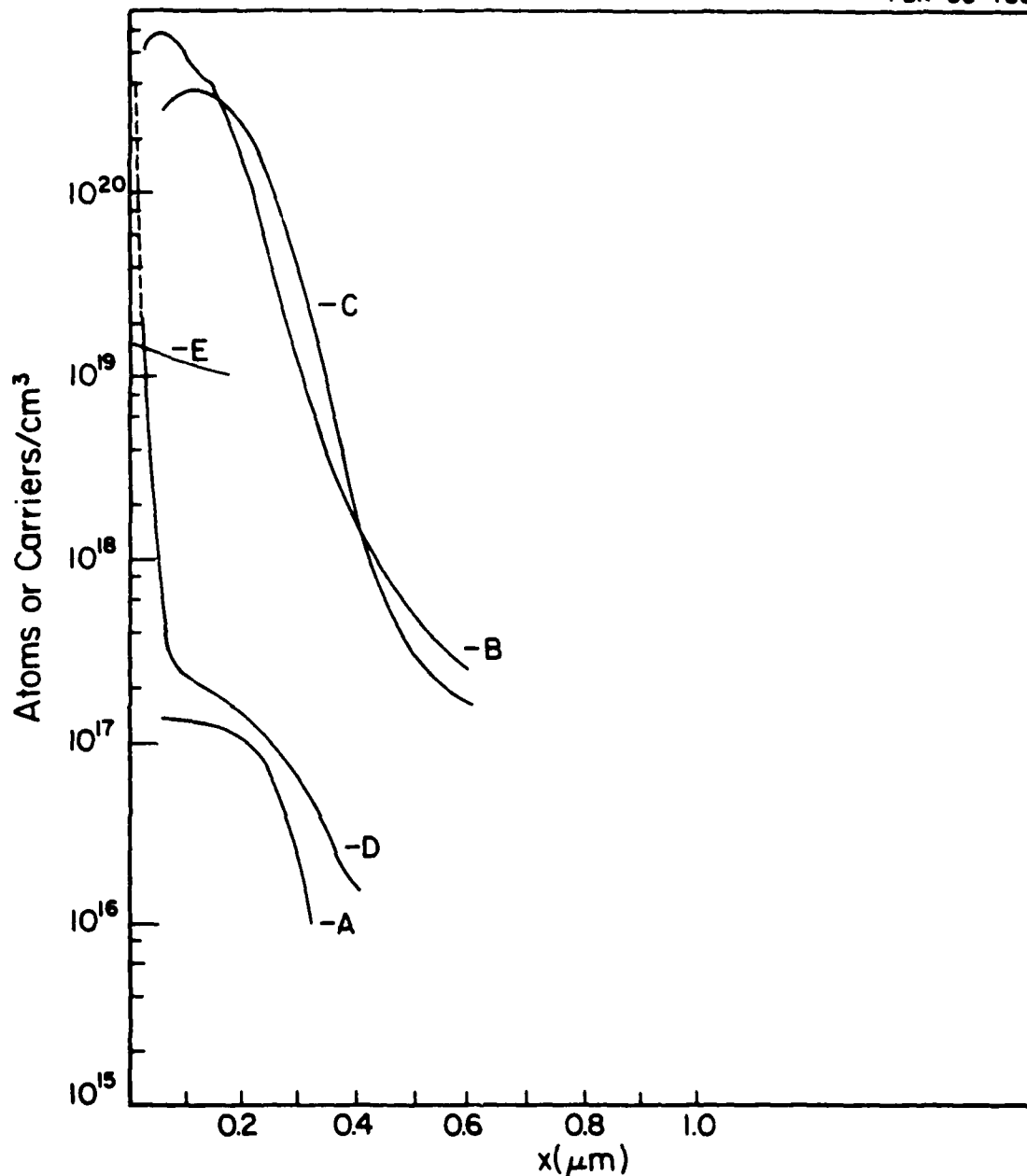


Figure 15. SIMS and carrier profiles. A: C-V carrier concentration profile of sample 7A25B as received. B: SIMS profile of 5×10^{15} Se/cm² at both 120 and 320 keV into semi-insulating GaAs. C: SIMS profile of the same Se implant in 3-7A25B-3 after PEBA. D: SIMS profile of Si in 3-7A25B-3 after PEBA. E: Carrier profile of the same implant in 2-41639-4 and 5.

Curve A of Fig. 15 is the carrier concentration from a C-V profile measured as part of the original epilayer characterization. Curve B is the selenium calibration run for the same implant into an undoped GaAs semi-insulating substrate obtained from Metals Research Corporation; this sample was not annealed and the profile is very similar to the profile calculated using LSS range statistics except for the tail extending beyond about 0.2 μm . Curves C and D are the selenium and silicon SIMS profiles of piece 3 following TiPtAu removal, and curve E is the differential carrier profile of sample 2-41639-4 and -5 taken from Fig. 14. Curves B and C indicate that there was relatively less selenium diffusion during PEBA for this deeper double-energy implant. The increased silicon concentration near the surface after PEBA is perhaps more interesting. Although that portion of the silicon curve above $2 \times 10^{19}/\text{cm}^3$ at the immediate surface is a SIMS artifact, the less steep portion down to about $2 \times 10^{17}/\text{cm}^3$ appeared on three PEBA pieces, 3-7A25B-1, 2, and 3, but was not present on the unannealed silicon implant calibration piece nor on a grown silicon-doped epilayer similar to the epilayer on 7A25B.

Aside from the PEBA anneal, the only difference in sample preparation was the deposition and removal of TiPtAu, which would not seem likely to introduce any silicon. It therefore appears that silicon has moved toward the surface in sufficient concentration to be important relative to the measured carrier concentration and there may be differences in the behavior of PEBA-implanted contacts in silicon-doped epilayers compared with semi-insulating substrates. That curve D is higher than curve A over the full depth is consistent with the fact that D is a measure of silicon atom concentration while A measures only the uncompensated carrier concentration.

Figure 13 shows the profiles of 2-41639-2 after a Si_3N_4 film was deposited and removed following PEBA. The nitride film was deposited in the cold-wall CVD reactor we use to deposit implant-anneal Si_3N_4 caps. The thermal cycle consisted of a 5 minute period at 200°C followed by a rise to 710°C and a 500-700 Å Si_3N_4 deposition, all in about 20 seconds, followed by a rapid cool to 200°C in less than one minute. The deposition takes place in flowing silane and ammonia diluted in nitrogen with the sample resting on a $3 \times 1 \times 0.4 \text{ in}^3$ graphite strip resistor heating element. This experiment was done because we considered depositing a Si_3N_4 passivation after PEBA in FET device processing, and it

showed that such a step would severely reduce the carrier concentration of the contacts.

Section 2-41639-3 of this sample was saved for contact resistance measurements, which will be discussed later.

2. Profiles with Reduced Implant Dose and PEBA Fluence

a. Reduced implant doses

Selenium implants of $5 \times 10^{15}/\text{cm}^2$ at both 120 and 320 keV had yielded peak concentrations in excess of $10^{19}/\text{cm}^3$, but these carrier concentrations integrated over the profile depth only represent a few percent of the total implanted dose. The great excess of unaccounted-for selenium, probably present in microprecipitates, could be detrimental in device contacts, so we wanted to establish whether reduced doses would be effective. Portions of epilayer wafers 3-7A17A and B were implanted at both 120 and 320 keV with selenium doses of 5×10^{14} , 1×10^{15} , and 4×10^{15} and PEBA-annealed at $0.71 \text{ J}/\text{cm}^2$. Differential carrier profiles of the latter two had peak concentrations above $10^{19}/\text{cm}^3$. Figure 16 shows that the profile (curve A) from the dual-energy implant at $5 \times 10^{14} \text{ Se}/\text{cm}^2$ peaks at only about $10^{17}/\text{cm}^3$. These results indicate that for the conditions described in this report a total dose of between 1 and $2 \times 10^{15} \text{ Se}/\text{cm}^2$ is required to achieve a carrier concentration in excess of $10^{19}/\text{cm}^3$. However, curves B and C show that the addition of dual silicon implants at 50 and 130 keV to the same $5 \times 10^{14} \text{ Se}/\text{cm}^2$ dual implant yields peaks above $10^{19}/\text{cm}^3$. Curve B results from added silicon implants of $5 \times 10^{13}/\text{cm}^2$ at both energies for a net Se + Si dose of $1.1 \times 10^{15}/\text{cm}^2$ and shows an increase of more than an order of magnitude in peak concentration for only a 10 percent increase in total dose. Curve C shows that a fourfold increase in the silicon dose has, if anything, reduced the number of carriers.

b. Reduced PEBA fluence

A $3.4 \times 4.9 \text{ cm}^2$ epilayer sample, 7B-118, was implanted with $5 \times 10^{15} \text{ Se}/\text{cm}^2$ at 120 keV and cleaved into four pieces. Sections 4-7B118-2, 3, and 4 were PEBA-annealed at fluences of 0.42, 0.50, and $0.59 \text{ J}/\text{cm}^2$ respectively. The four-point probe sheet resistances of these pieces and 1-41614-8 are shown in Fig. 17. Profile measurements revealed peaks $\gtrsim 10^{19}/\text{cm}^2$ for all these samples.

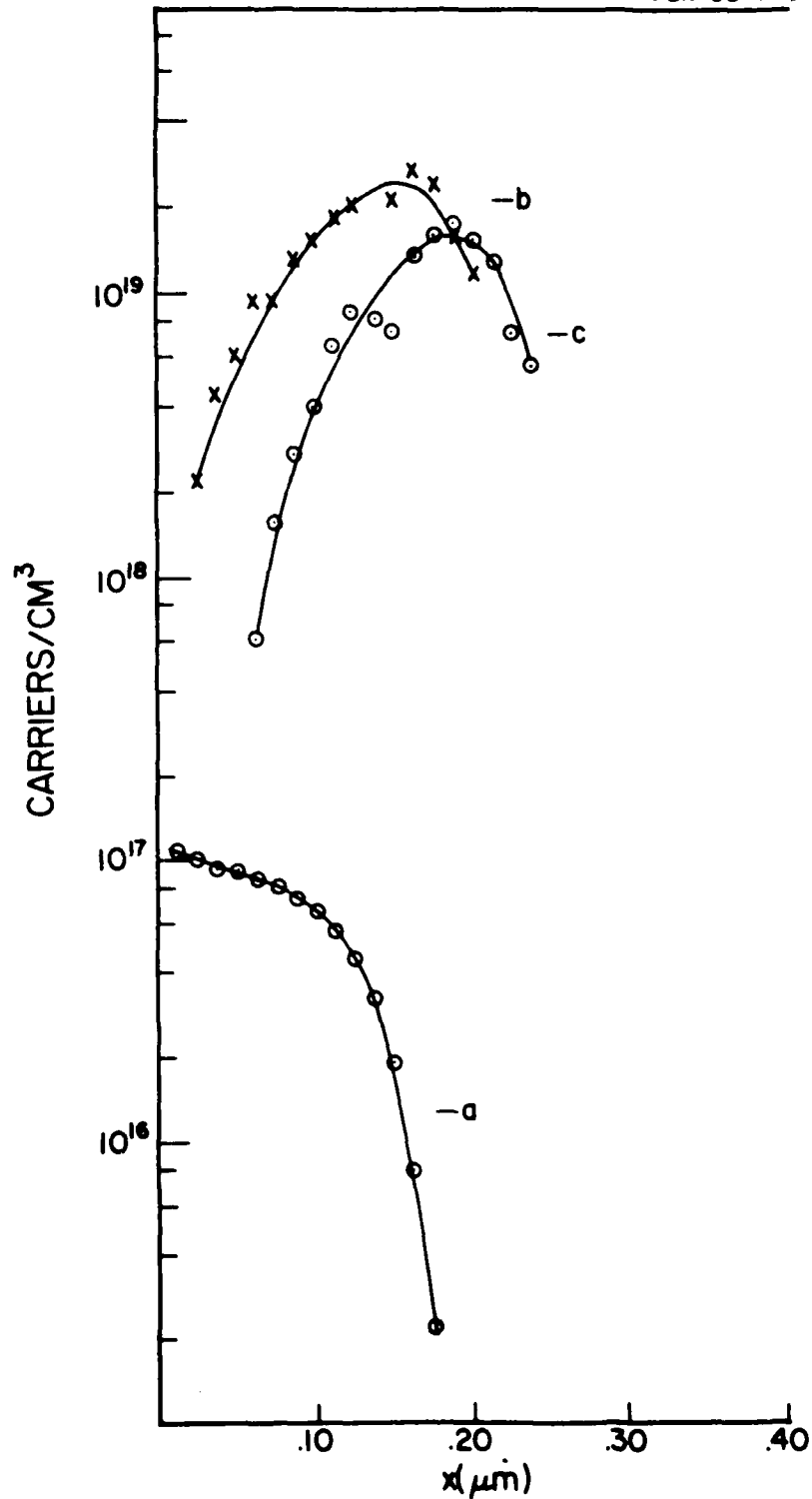


Figure 16. Carrier profiles for PEBA Se implants of $5 \times 10^{14}/\text{cm}^2$ at both 120 and 320 keV (a) plus additional Si implants of $5 \times 10^{13}/\text{cm}^2$ (b) and $2 \times 10^{14}/\text{cm}^2$ (c) at both 50 and 130 keV.

PBN-80-653

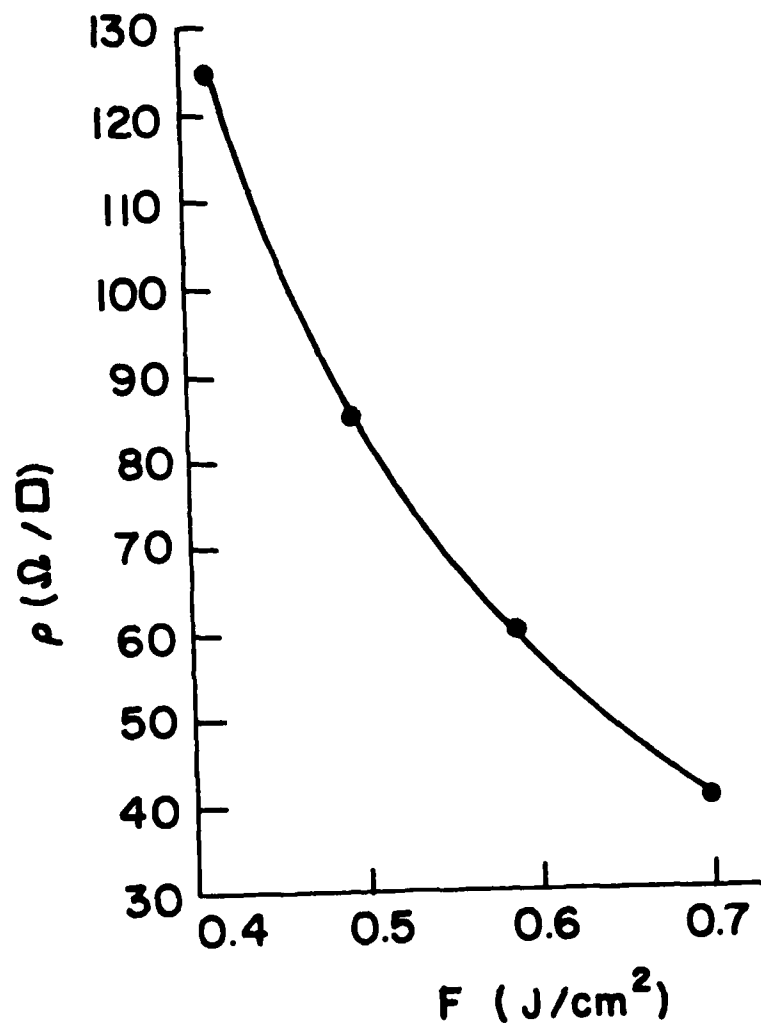


Figure 17. Sheet resistances of a PEBA Se implant as a function of PEBA fluence.

To see what effect this range of fluences would have on an unimplanted epilayer, Samples 3-7A91-1, 2, 3, and 4 were PEBA-exposed with fluences 0.21, 0.31, 0.59, and 0.84 J/cm², respectively. Figure 18 shows the C-V carrier profiles prior to PEBA and after a PEBA of 0.59 J/cm² on section 3, and 0.84 J/cm² on section 4.

Sections 1 at 0.21 J/cm² and 2 at 0.31 J/cm² were barely affected except that the zero bias capacitance decreased from 146 pF to 116 pF for section 1 and 107 pF for section 2 compared with 45 pF for section 3, indicating some small loss of carriers within about 0.2 μm of the surface.

The fact that a very narrow range of fluences from 0.4 to 0.6 J/cm² might yield a high enough carrier concentration to form unalloyed ohmic contacts without completely destroying unimplanted channel-type layers offers some hope that an unprotected sample with localized contact implants in a device configuration might be successfully PEBA-annealed. We explored this possibility in the last exposure set.

c. Contact resistances and thermal stability

Sample 2-41639-3, implanted with 5×10^{15} Se/cm² at 120 keV, was intended to be used for contact resistance measurements. It broke approximately in half during transport from Raytheon to Spire Corporation and the two halves, A and B, were mounted adjacent to one another and annealed with 0.67 J/cm². Four-point probe checks showed about 47 ohms/sq on A and 29 ohms/sq on B.

We felt it would be best to have the metal-GaAs interface near the peak of the carrier concentration, so using the carrier profile from 2-41639-1 (Fig. 12) as a guide we removed about 750 Å of the surface. This was done by ion milling since we were confident of its accuracy in layer removal. The resistances were then 75 and 40 ohms/sq. for the thinner layers. Contact resistance patterns were then opened in AZ1350 resist and piece A was given a 15 second damage removal etch in H₂O₂-NH₄OH (pH ≈ 7). Both A and B were rinsed in 5 percent NH₄OH and immediately loaded into an evaporation system for deposition of

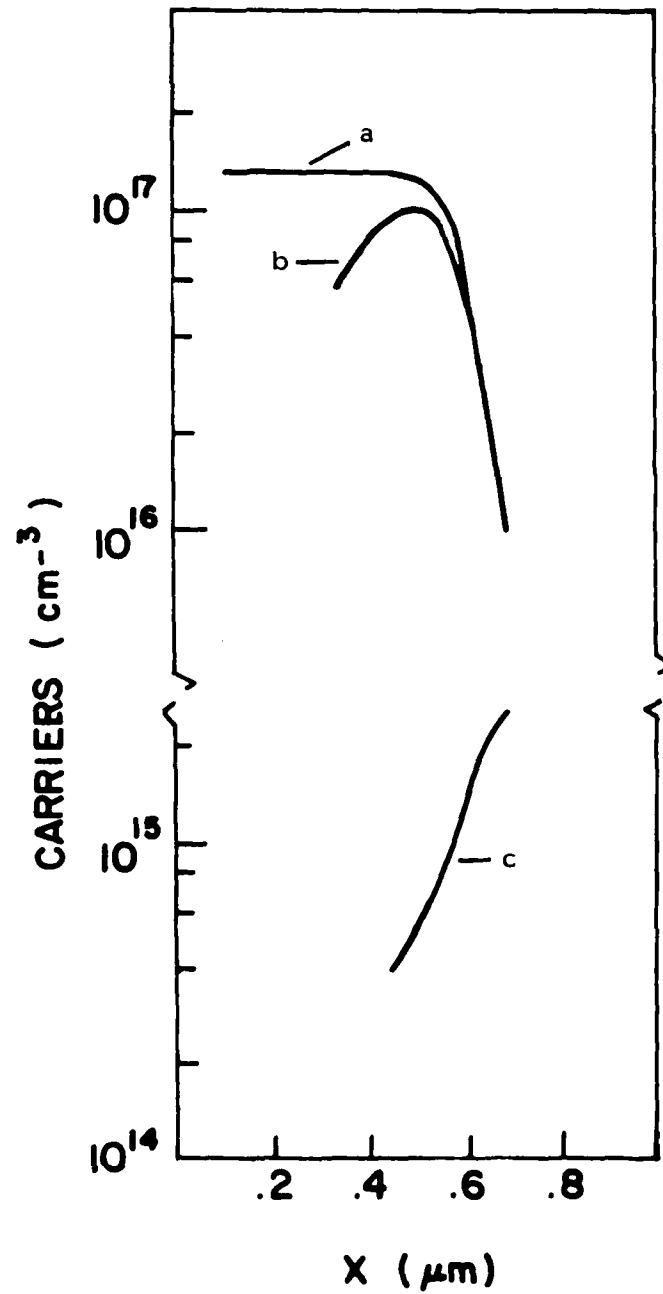


Figure 18. C-V measured carrier profiles after PEBA with fluences of b) 0.59 J/cm^2 and c) 0.84 J/cm^2 compared with a) the original epilayer profile.

1000, 1000, 3000 Å of TiPtAu. The patterns were then completed by resist liftoff and mesa etch isolated by ion milling with an AZ1350J resist mask protecting the patterns.

Measurements on many patterns on both pieces yielded specific contact resistivities r_c and sheet resistance R of:

Piece A	$r_c \approx 3 \times 10^{-7} \text{ ohm cm}^2$	$R = 74 \text{ ohms/sq.}$
Piece B	$r_c \approx 3 \times 10^{-5} \text{ ohm cm}^2$	$R = 31 \text{ ohms/sq.}$

The value for piece A was the lowest ever reported²⁴ for GaAs and comparison with piece B, which had a lower sheet resistance but much higher contact resistivity, demonstrated the importance of proper surface preparation prior to metal deposition.

The thermal stability of these remarkably low contact resistances was in question, however, because the peak carrier concentration and sheet resistances of uncovered surfaces had proven to be considerably degraded by relatively mild heat treatments typically used in alloying NiAuGe contacts. To determine what might happen to the atomic distribution under TiPtAu metallization, samples 3-7A25B-1 and 2 were coated with TiPtAu after PEBA implant; sample 1 was heated at 150°C for 24 hours and sample 2 at 250°C for 24 hours. The metallization was removed and SIMS profiles were measured and compared with an unannealed sample, 3-7A25B-3 (see Fig. 15). No selenium or silicon profile changes were seen.

The effect of heating on contact resistance was measured on samples 3-7A22A and 3-7A22B. These were n-type epilayers implanted with $5 \times 10^{15} \text{ Se/cm}^2$ at both 120 and 320 keV and PEBA-annealed at 0.67 J/cm^2 . TiPtAu contact resistance patterns were deposited without ion milling and only 10 sec in HCl, 30 sec in H_2O_2 - NH_4OH and a 5 percent NH_4OH rinse for predeposition preparation of the surface. Table IV shows the effect of heating these samples.

These values represent averages over many patterns, for example 39 for sample 7A22A, where only those data with correlation coefficients $r \geq 0.9995$ were

TABLE IV

<u>Sample</u>	<u>Anneal</u>	<u>r_c (ohm cm^2)</u>	<u>R (ohms/sq.)</u>
7A22A	None	$1.5 \cdot 10^{-6}$	25
7A22A	150°C in vacuum, 8 Hrs.	$3 \cdot 10^{-7}$	34
7A22B (7B158)	None	$2 \cdot 10^{-6}$ ($1.2 \cdot 10^{-6}$)	40 (61)
7A22B (7B158)	4 hrs. in H_2 at 250°C	$6 \cdot 10^{-7}$ ($1.74 \cdot 10^{-6}$)	63 (62.2)
7A22B	8½ hrs. in H_2 at 250°C	$6 \cdot 10^{-7}$ ($2.22 \cdot 10^{-6}$)	63 (63.0)

included. These data show that, whereas the sheet resistance of the uncovered gaps between TiPtAu contacts increased with heating, the contacts actually improved with heating. As will be shown later, this was not the case for unalloyed contacts on highly doped grown epilayers.

For comparison with our standard NiAuGe alloyed contacts, the results of annealing sample 7B158 are shown in parentheses. This sample had a highly doped surface 0.2 μm thick with about 10^{19} carriers/ cm^3 at the immediate surface above a 0.45 μm layer with 9.6×10^{16} carriers/ cm^3 grown on a 2.0 μm buffer layer. The R and r_c values for 7B158 are for a typical contact resistance pattern, and although there was some variation in values over the wafer, the percentage changes in R and r_c after 4 hours at 250°C were consistently close to 2 percent and 45 percent respectively. After a total of 8½ hours the increases in R and r_c were 3 percent and 85 percent respectively.

d. Effects of discontinuous topography

It was clear from the first exposure set that unimplanted, unprotected epilayers would probably not survive PEBA. In the next set we therefore tried to determine what thickness of two convenient protective layers, SiO_x and photoresist, if completely covering the surface, would preserve the electrical characteristics of an underlying n-type epilayer. Prior to PEBA, a narrow section

was cleaved off the side of a wafer and C-V carrier profiles were measured. The remaining piece was coated, PEBA annealed, stripped of its protective coat, and C-V profiled for comparison with the unannealed piece. The fluence was 0.71 J/cm^2 and the blocking layers were $1\frac{1}{4}$, $2 \text{ }\mu\text{m}$ of AZ1350J resist and 0.5 , $0.75 \text{ }\mu\text{m}$ of SiO_x .

Visual inspection following PEBA revealed that the thinner resist was removed except for a residue of microscopic spots and that the thicker resist was removed over part of the wafer. SiO_x coatings appeared unaffected except for removal near the edges of the $0.5 \text{ }\mu\text{m}$ film. CV profiles of several Schottky diodes formed on each piece showed that each mask except the $0.5 \text{ }\mu\text{m}$ SiO_x film offered sufficient protection for FET channels.

Three epilayer samples with windows opened in contact regions and selenium implanted in PFET and contact resistance test patterns were also PEBA annealed in this set. The following protective layers were present except over the contact regions:

<u>Sample</u>	<u>Bottom Coating</u>	<u>Top Coating</u>
2-72676	$700\text{--}1000 \text{ }\overset{\circ}{\text{A}}$ Si_3N_4	$2.2 \text{ }\mu\text{m}$ AZ1350J
2-41633-1	$700\text{--}1000 \text{ }\overset{\circ}{\text{A}}$ Si_3N_4	$0.9 \text{ }\mu\text{m}$ SiO_x
2-41633-2	$700\text{--}1000 \text{ }\overset{\circ}{\text{A}}$ Si_3N_4	$0.9 \text{ }\mu\text{m}$ SiO_x

After the PEBA exposure of a batch of five samples, including 2-72676 but not 2-41633-1 and 2, we found that the tungsten filament in the electron beam system had burned out during the run and although it was evident that the samples had received some exposure it was not possible to tell how much. They were therefore pulsed a second time.

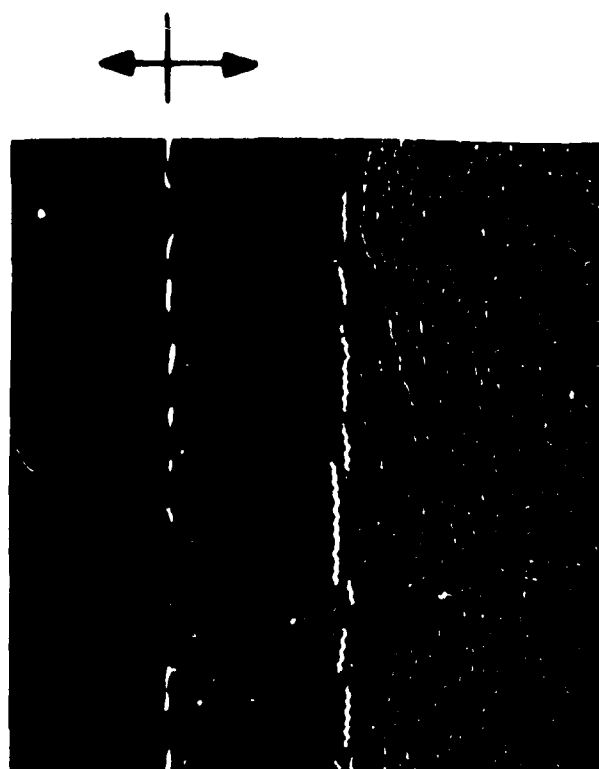
Following PEBA, about $750 \text{ }\overset{\circ}{\text{A}}$ was ion milled off the contact regions: about $300 \text{ }\overset{\circ}{\text{A}}$ more was removed in a chemical etch. A rinse in 5 percent NH_4OH was followed by deposition of $1000 \text{ }\overset{\circ}{\text{A}}$ Ti, $1000 \text{ }\overset{\circ}{\text{A}}$ Pt, $3000 \text{ }\overset{\circ}{\text{A}}$ Au on the contacts. Non-ohmic behavior was observed on 2-72676 and the SiO_x masked pieces were effectively nonconducting. This showed that a patterned sample with masked, unim-

planted areas adjacent to unmasked, implanted areas responds differently to PEBA than a uniform surface of either type.

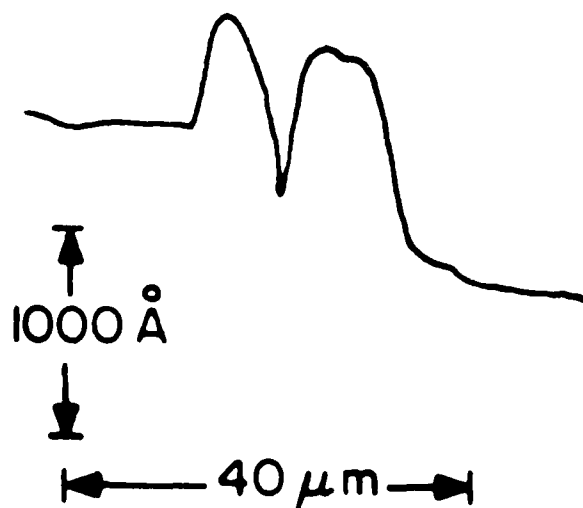
To observe the effects of a simple boundary on a larger scale than is possible in a device pattern, a window about 1 cm^2 was opened on sample 3-7A90-1. The rest of the sample was coated with $3/4\text{ }\mu\text{m}$ of SiO_x and $2\text{ }\mu\text{m}$ of AZ1350J. About $0.08\text{ }\mu\text{m}$ of GaAs was etched in the window to delineate the boundary and the sample was implanted with $5 \times 10^{15}\text{ Se/cm}^2$ at both 120 and 320 keV. The resist was then removed and the sample was exposed to PEBA. Fig. 19a is a dark-field photograph of the boundary after PEBA and freon plasma etch removal of residual SiO_x . A transition strip over $20\text{ }\mu\text{m}$ wide appears between the masked portion at the left and the unmasked region at right. The white specks at right are the gallium residues typically seen on bare GaAs after PEBA. Figure 19b is a Dektak trace across the transition region that shows surface ripples as high as $0.1\text{ }\mu\text{m}$, suggesting that the electron-beam-heated GaAs expanded upward where it was restricted by GaAs shielded from both selenium ions and electron heating. Figure 20 is a SEM photograph of the transition region. This extended and distorted boundary region makes it questionable whether selectively masked PEBA annealing will be useful for FET structures.

The last attempt made to assimilate PEBA into power-FET fabrication was to expose the narrow range of PEBA fluences which might activate implanted contacts without destroying channel layers. Samples with rather thick n-type epilayers doped with $10^{17}\text{ carriers/cm}^3$ were chosen for this experiment. Sample 7B110A was a $2.4 \times 3.4\text{ cm}^2$ slice with a $0.8\text{ }\mu\text{m}$ n-type layer over a $2\text{ }\mu\text{m}$ buffer layer. Sample 7B118 was $3.4 \times 4.9\text{ cm}^2$ with a $0.5\text{ }\mu\text{m}$ n-type layer and a $2\text{-}\mu\text{m}$ buffer layer. Sample 7B118 was divided into four pieces, three of which were used to measure peak carrier concentrations at reduced fluences, as previously discussed, and sample 7B110A was cleaved in half. A source-drain power-FET pattern was opened in $2\text{ }\mu\text{m}$ of AZ1350J, about $0.05\text{ }\mu\text{m}$ of GaAs was etched off to delineate the pattern, and the samples were implanted with $5 \times 10^{15}\text{ Se/cm}^2$ at 120 keV. After stripping the resist, samples 4-7B118-1 and 4-7B110A-1 and 2 were PEBA-annealed at 0.42, 0.50, and 0.59 J/cm^2 , respectively. Following PEBA and the usual HCl dip, samples had the textured appearance shown in Fig. 21a in the

Masked PEBA Implant



a



b

Figure 19. (a) Photograph of boundary region (610x) showing masked region (left) and annealed implant region (right); (b) Dektak trace across boundary with scales indicated.

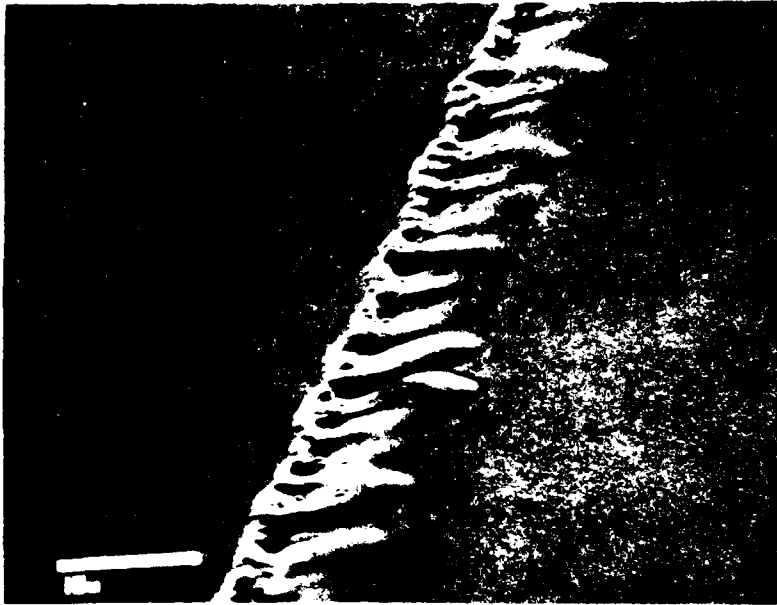
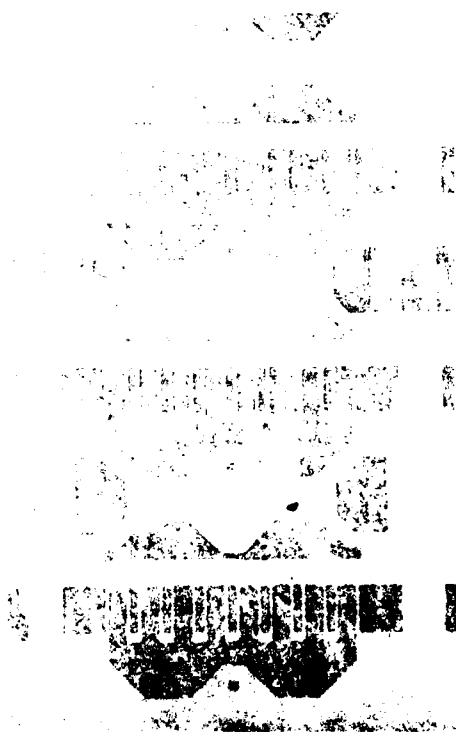


Figure 20. SEM photo of the transition region on 3-7A90-1 between the masked portion at left and the PEBA implant at right after removal of the SiO_x and gallium residues.

PBN-80-796



(a)

Figure 21. a) Optical photograph at 64X of 4-7B118-1 after a localized implant in the device pattern and an unmasked PEBA; b) Two alignment squares opened and implanted with the source-drain pattern.



(b)

implanted source-drain regions. Figure 21b is a SEM photograph of two mask alignment squares opened and implanted along with the source-drain pattern. Although implanted regions appear to be rougher at low magnification in Fig. 21a, the SEM pictures reveal that aside from craters the surface has a smooth appearance characteristic of a recrystallized melt surrounded by a nonabrupt, nonflat boundary and relatively rough unimplanted environs.

The degree of texturing was nonuniform in appearance over the surface of each of the three samples with this pattern. It had not been observed on the other sections of 7B118 which were blanket implanted and annealed nor on any previous samples, including those having the same pattern, with regions other than the source and drain contacts masked with SiO_x or AZ1350J. The relative importance of the implant and the $0.05\text{ }\mu\text{m}$ recess in producing this texture is unknown since they were not tried separately. A more drastic result of PEBA-implant is shown in Fig. 22. This epilayer sample 3-7A91-6 was a PEBA following an implant of $5 \times 10^{15}\text{ Kr/cm}^2$ at both 120 and 320 keV. The unmarred portion of the sample is a corner which was masked from the implant by the wafer holder. Krypton apparently erupted out of the surface during PEBA.

TiPtAu metallization was evaporated on the source-drain regions of the patterned samples by remasking with resist which was removed after metal evaporation to lift off unwanted metal areas.

Sample 4-7B110A-2 which had the highest PEBA fluence had a moderate yield of ohmic contacts in some test pattern areas and this sample was continued through gate metallization but no encouraging FET characteristics were obtained. Hardly any ohmic contacts were found on the samples with lower PEBA fluence.

PBN-80-793



Figure 22. SEM photos of 3-7A91-6. The lower right portion was masked from the Kv implant by the implant sample holder.

SECTION IV

FURNACE ANNEALED CO-IMPLANTS OF SELENIUM AND SILICON

At the suggestion of our contract monitor, Mr. Max Yoder, we implanted, according to the following two schedules, sections of wafer 7A86 which had a 0.5 μm n-type layer doped at $1.2 \times 10^{17}/\text{cm}^3$ over a 2 μm thick buffer layer.

Type 1

4.45×10^{13}	Se/cm ²	-	120 keV
1.0×10^{14}	Se/cm ²	-	320 keV
5.0×10^{13}	SiH/cm ²	-	50 keV
1.15×10^{14}	SiH/cm ²	-	130 keV

Type 2

The same schedule as Type 1 but with all the doses doubled.

The samples were then coated with Si_3N_4 and annealed in flowing nitrogen at 815°C for thirty minutes. The implants were designed to yield matched Si-Se profiles with the selenium concentration about 15 percent less than silicon and the anneal was kept below 825°C to inhibit the formation of self-compensating Si-Si complexes.

The calculated profiles based on (LSS) range statistics assuming one carrier for each silicon and selenium ion and the measured profiles are shown in Fig. 23. The profiles were measured using resistance measurements at 125 \AA thick layer removal intervals and Hall measurements at 1250 \AA intervals. Concentrations in excess of $10^{19}/\text{cm}^3$, which would be required for unalloyed contacts, were not obtained on this first attempt and no other attempts were made.

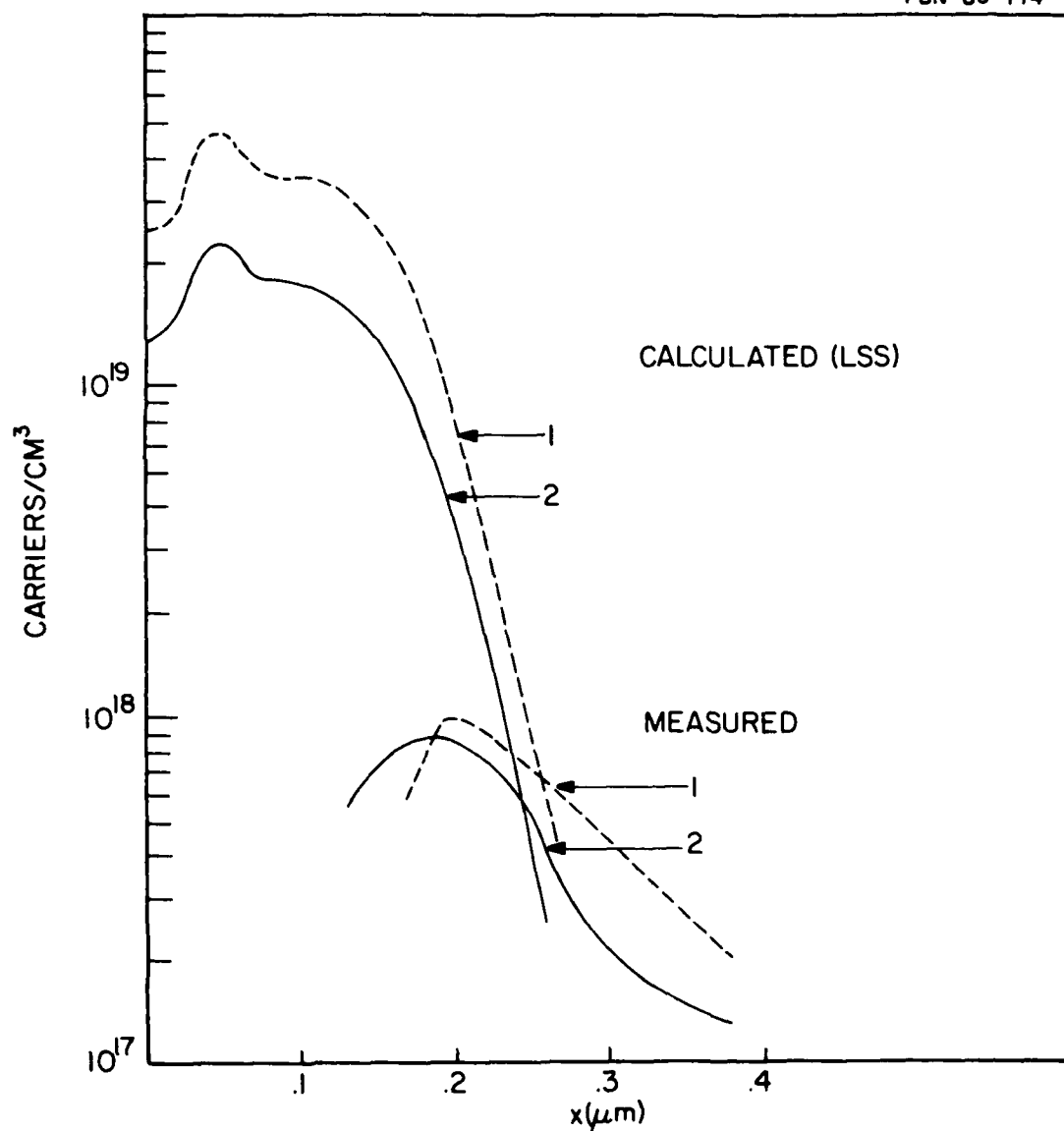


Figure 23. Calculated and measured profiles for furnace annealed Se-Si implants. Sample 1 - 8.9×10^{13} Se/cm² (120 keV), 2.0×10^{14} Se/cm² (320 keV), 1×10^{14} Si/cm² (50 keV), 2.3×10^{14} Si/cm² (130 keV). Sample 2 - same as sample 1 but at half the dose.

SECTION V

HIGHLY DOPED GROWN EPILAYER SURFACES

A. CARRIER PROFILES

Contact layers are formed in our vapor-phase epitaxy reactor during the last minute of epilayer growth by increasing the silane flow, reducing the mole fraction of arsenic trichloride in the gas stream, and then pulling the furnace away from around the gallium source to reduce the gallium vapor pressure. Epilayers grown this way have concentrations exceeding 10^{19} carriers/cm³ at the immediate surface but dropping very sharply so that the depth over which the concentration exceeds 10^{19} /cm³ is not much greater than the zero-bias depletion depths of $\lesssim 70 \text{ \AA}$ estimated from capacitance measurements. Profiles of a sample grown at the beginning of this study are shown in Fig. 24.

Unalloyed contacts deposited on these layers cover a broad range of specific contact resistances from $8 \times 10^{-6} - 10^{-4} \Omega\text{cm}^2$ and the contacts were not always ohmic. We therefore tried to grow thicker layers having over 10^{19} carriers/cm³. First the time t , during which the silane flow is increased and the arsenic trichloride mole fraction is reduced, was increased to $2t$, $4t$, and $6t$, where $t = 10$ seconds. As shown in Fig. 25, this produces an increase in the thickness of the transition layer between the surface and a channel-type layer but does not achieve the desired result of increasing the surface layer thickness.

The second approach was to vary the duration of a brief pause, prior to retracting the furnace, during which the inflow of arsenic trichloride was terminated. Fig. 26 shows the profile measured on a typical sample, 7B166B. Once again the transition layer was altered, but the depth of the 10^{19} /cm³ layer is about the same.

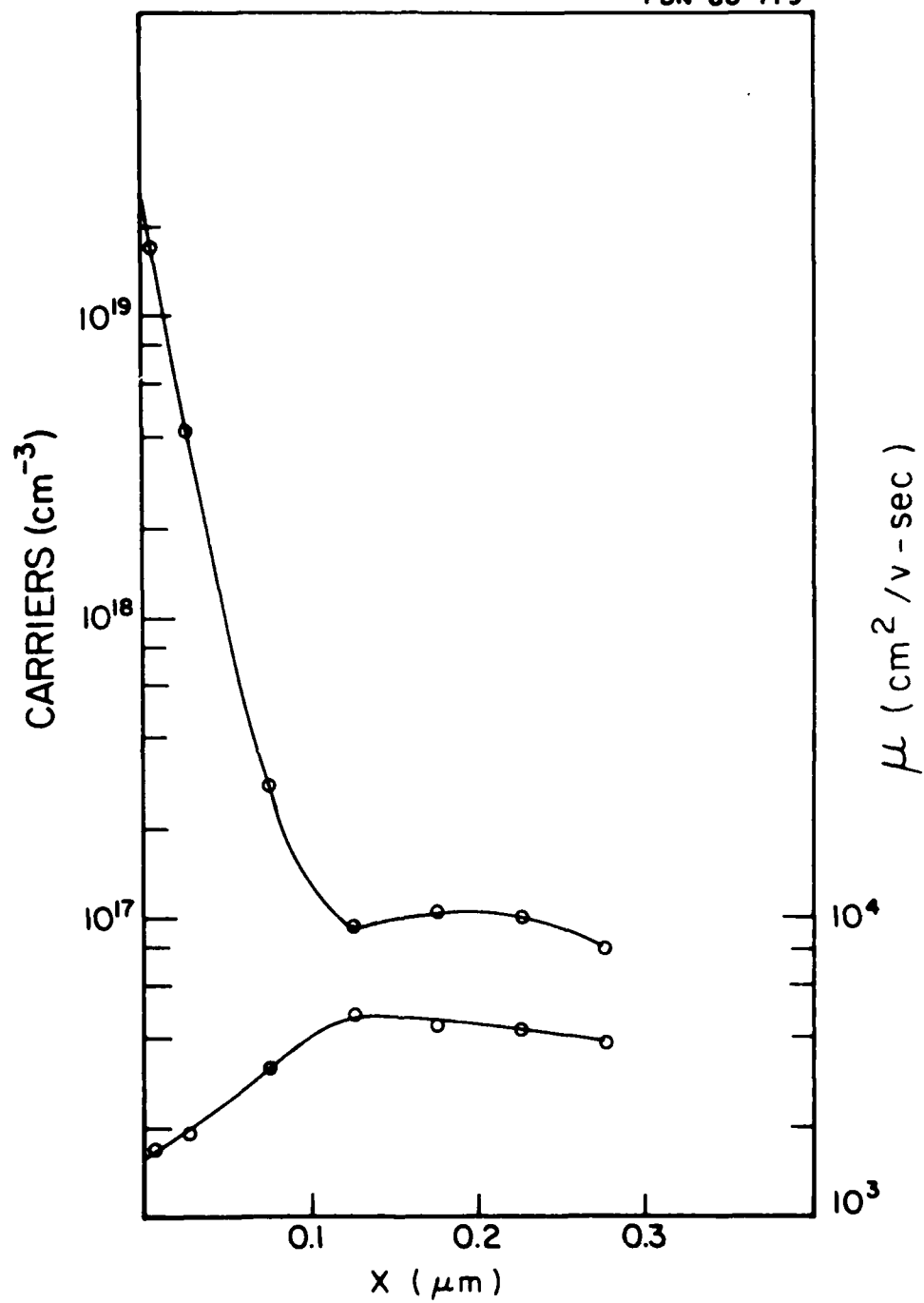


Figure 24. Carrier and mobility profile of a grown epilayer having an n^{++} surface.

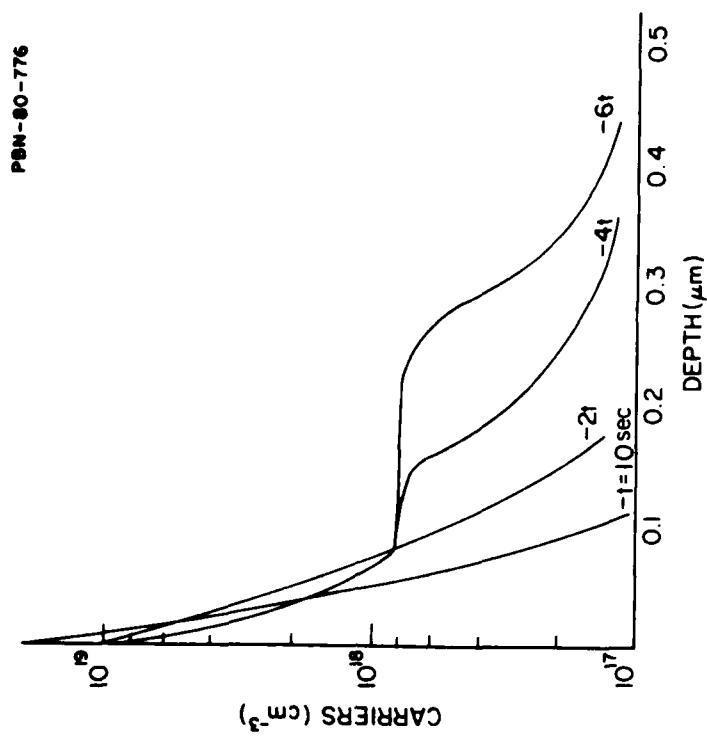
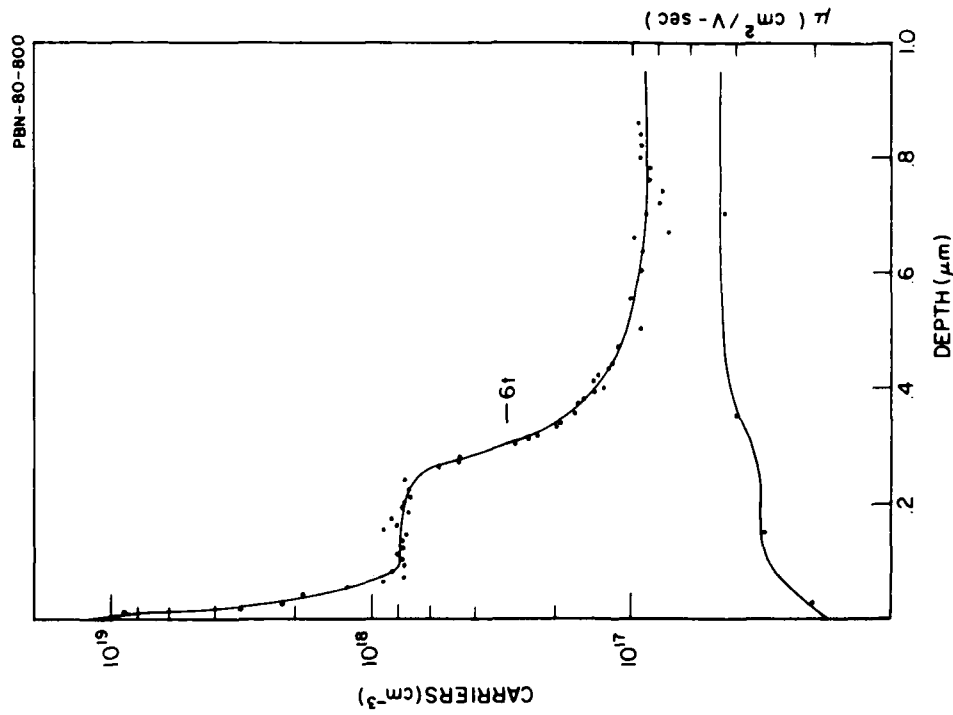


Figure 25. Carrier concentration profiles for increased silane flow times. For clarity, experimental points are omitted on the composite graph.

This is shown by the electrical and SIMS profiles of two different samples grown this way (Fig. 26). Thus far we have not been able to grow thicker layers having over 10^{19} carriers/cm³.

The profiles in Figs. 24-26 were obtained using ion milling for removal of 125 Å thick layers. As mentioned previously, this technique may yield an erroneously high concentration value at the immediate surface. As a check, we therefore measured the zero-bias capacitance C_0 of Shottky diodes deposited on these samples. Values above 2000 pF were measured for 16 mil diameter diodes, and the formula

$$N = \frac{2\phi_B (C_0/A)^2}{qKE}$$

where $\phi_B \approx 0.9$ volts, built-in voltage

A = diode area

$q = 1.6 \times 10^{-19}$ coulombs

$K = 12$, dielectric constant of GaAs

$E = 8.86 \times 10^{-14}$ f/cm, free space permittivity

confirms that carrier concentrations were over 10^{19} /cm³.

B. CONTACT RESISTANCES AND THERMAL STABILITY

Samples were prepared to study the effects of heating in the same way as previously described for PEBA-annealed contacts, except that no surface removal was made aside from an NH₄OH rinse immediately before vacuum loading for TiPtAu deposition. SIMS profiles of sample 7B129A, one section unannealed after TiPtAu deposition and the other section annealed in hydrogen for 24 hours at 250°C, showed no measurable difference in silicon profiles. Table V shows the changes induced by heating contact resistance patterns on samples from wafer 7B166 whose carrier profile is shown in Fig. 26. Note that, in contrast with PEBA-implanted contacts, the sheet resistance is unaffected but the contact resistance degrades with heating. Unfortunately, the sample chosen for this test did not happen to be one of the ones with a lower contact resistance to begin

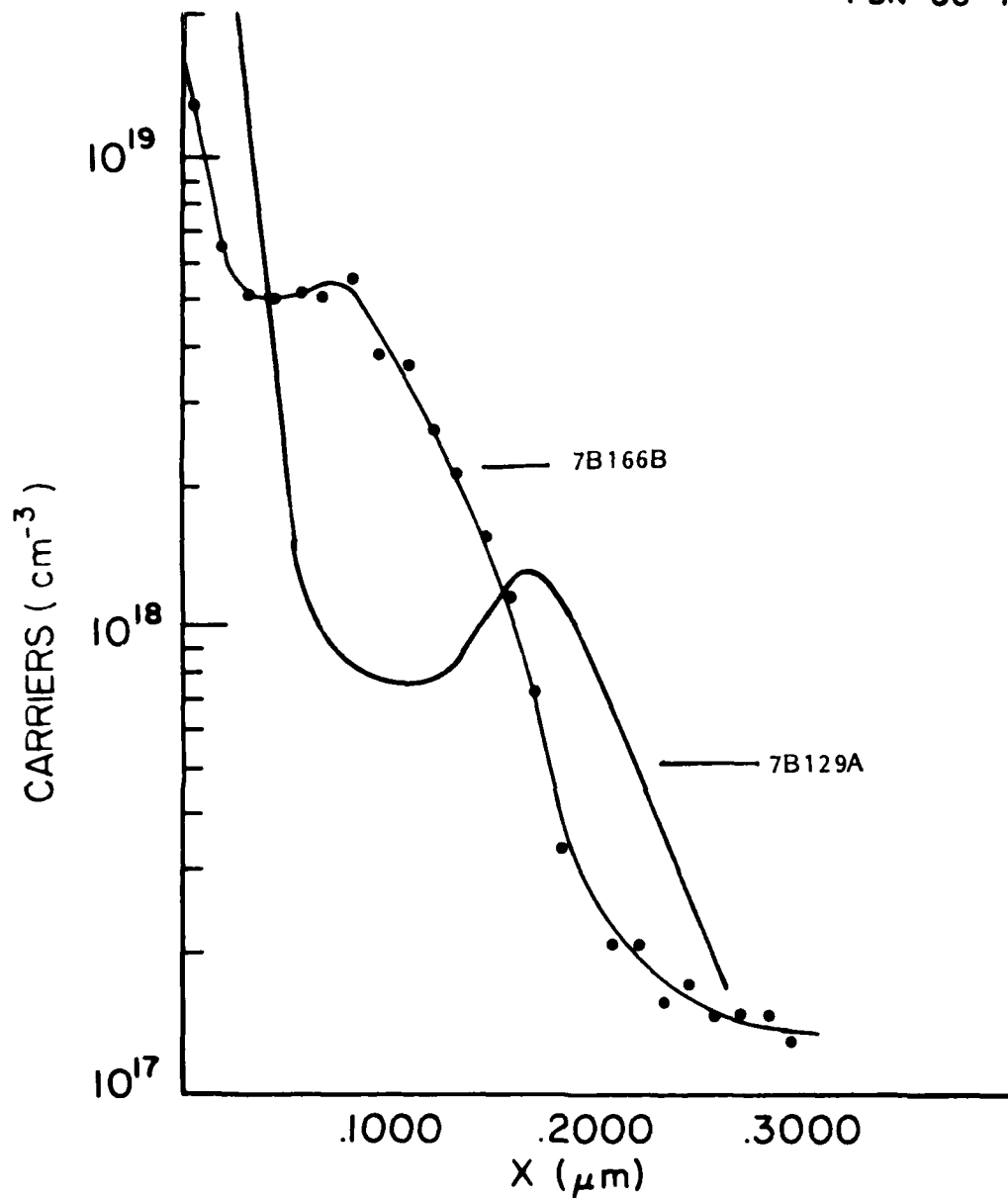


Figure 26. Electrical profile of epilayer 7B166B and SIMS profile of epilayer 7B129A.

with and the thermal behavior may not be representative of the lower resistivity samples or of samples with thicker surface layers.

TABLE V

<u>Anneal</u>	<u>r_c (ohm/cm²)</u>	<u>R (ohms/sq.)</u>
None	9.6×10^{-5}	43
4 Hrs at 250°C	1.3×10^{-4}	43
4½ Hrs more at 250°C	1.7×10^{-4}	43

C. POWER FETS WITH UNALLOYED CONTACTS

Power FETs with unalloyed TiPtAu contacts and gates were made on epilayer wafers 82625 and 7B-218A, which had the following specifications:

	<u>Carrier Conc. (cm⁻³)</u>	<u>Thickness (μm)</u>
Immediate surface	$\geq 10^{19}$	---
Contact layer	$> 2 \times 10^{18}$	0.2
Channel	8.2×10^{16}	0.7 on 82625 0.4 on 7B-218A
Buffer	$\sim 5 \times 10^{13}$	2.0

Figure 27 shows a top view SEM photograph of the device structure made on wafer 82625 and a cross-sectional schematic of an FET cell. This device has 16 gates with gate lengths about 1.5 μm and a total periphery of 1.6 mm. The back side had TiAu (400, 5000 Å) soldered to a dogbone support and heatsink.

Wafer 7B-218A had a similar but improved design with 0.8 μm gate lengths and source contacts made through via holes from the back side, which was coated with TiAu (400, 5000 Å) followed by an additional 12 μm of gold plate. Devices were bonded to carriers by a very thin coat of a silver-filled epoxy, Epo-Tek H20E. Cantilever bonds to the gate and drain pads, which were formed during front-side processing, extended beyond the 4 mil thick

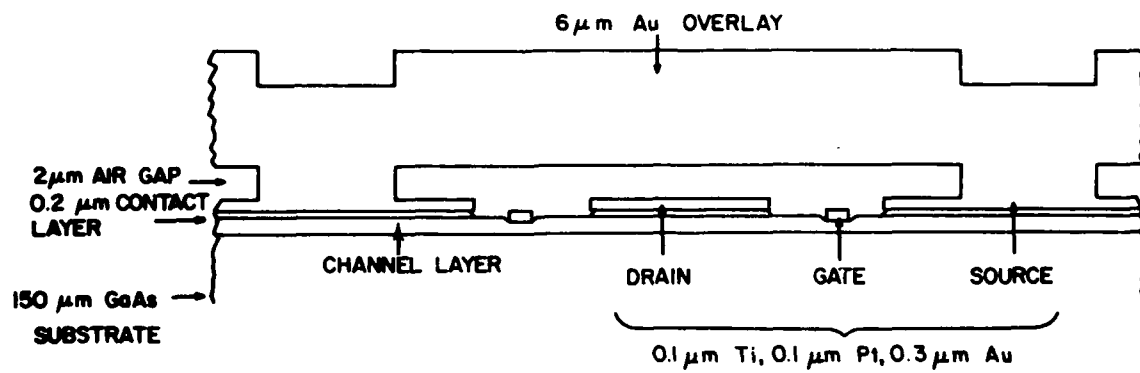
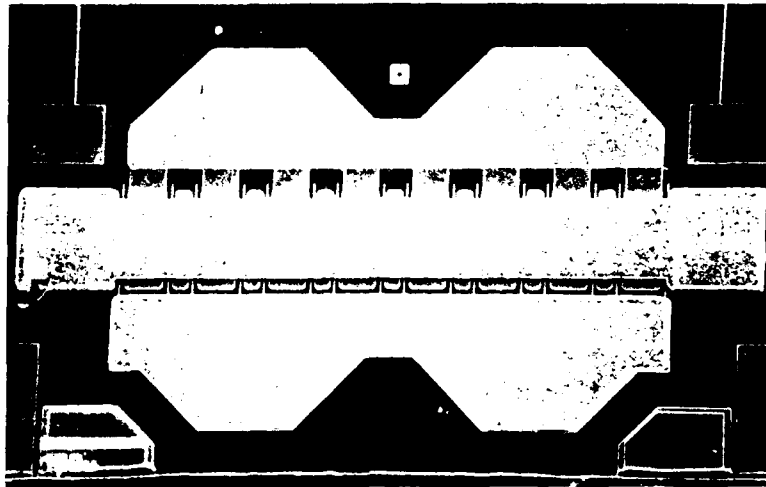


Figure 27. SEM photo of power FET and cross-sectional schematic of an individual cell.

GaAs chip and were thermocompression bonded to the chip carrier, which in turn was mounted in the jig shown in Fig. 28.

1. DC Characteristics

Saturation currents of devices from the two wafers were in the range of 230 to 350 mA with pinchoff voltages of 3 to 4 V. Drain currents were highly linear below saturation except very near zero drain voltage; and gate-drain leakage was low, for example less than 1 μ A at 12 V on devices from wafer 82625. Typical I-V characteristics are shown in Fig. 29. Ohmic contact resistances R_s and R_d were evaluated from measurements using various gate biases²⁶ and were in the range $1.5 \leq R_s + R_d \leq 2.4 \Omega$. These values are also typical of alloyed contacts made on the same type of device.

2. RF Measurements

The test jig was first calibrated by itself, using short and through-line samples (Fig. 30). Using the short sample, the reference planes were moved to the edge of the microstrip lines, while the through line data determined the loss in the jig. Measured S-parameters of FETs were corrected for the loss and the reference planes of the jig. Lead wire inductances were also de-embedded from the data. Maximum available gains, G_{max} were calculated from the S-parameters.

Output power performance was measured using the setup shown in Fig. 31. Input power was monitored by power meter 3 while output power was indicated by the differential volt meter which read the difference of the two power meters 1 and 2. Input and output tuners were always adjusted for the maximum power condition.

Examples of the S-parameters, G_{max} , and the input versus output power characteristics for a device from wafer 7B-218A are shown in Figs. 32, 33 and 34. G_{max} was 6.5 dB at 10 GHz, the small signal gain was 7.5 dB and the saturation power 0.5 W. The best result was obtained for a sample from wafer 82625 which was able to operate with a drain bias of 12 V.

804096C

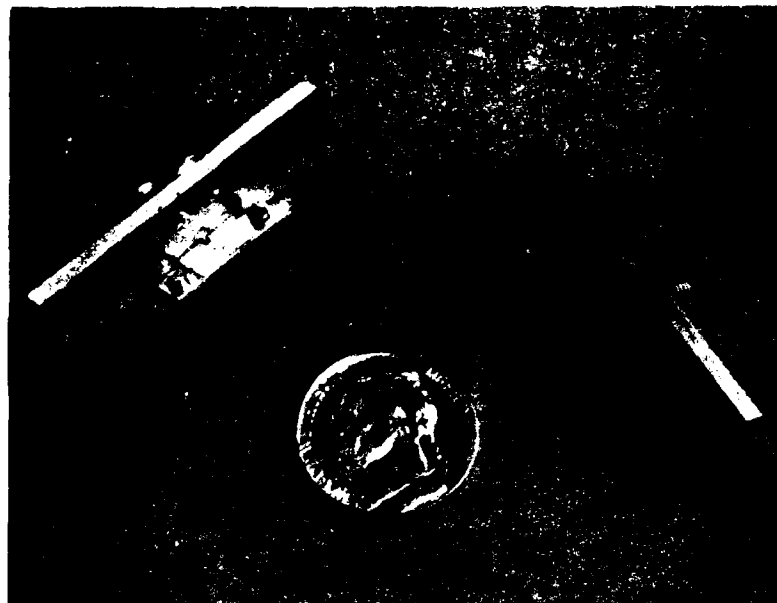


Figure 28. Test fixture used for electrical measurements.

PBN-80-1029

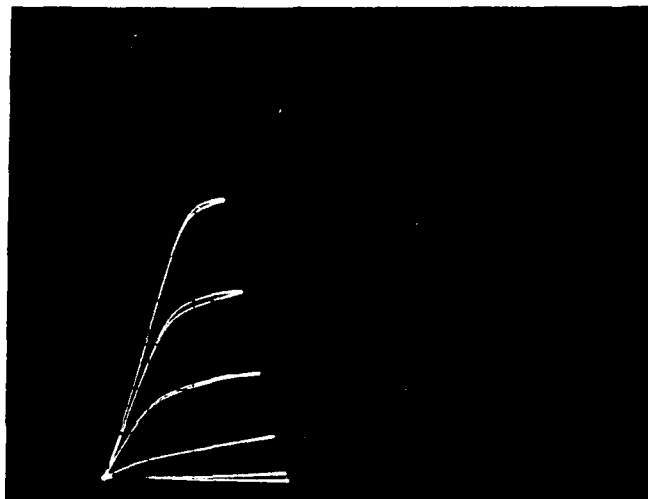


Figure 29. IV curves of an unalloyed contact power FET from wafer 7B-218A. Scales are 50 mA per vertical division, 1V per horizontal division. Gate steps are 1V.

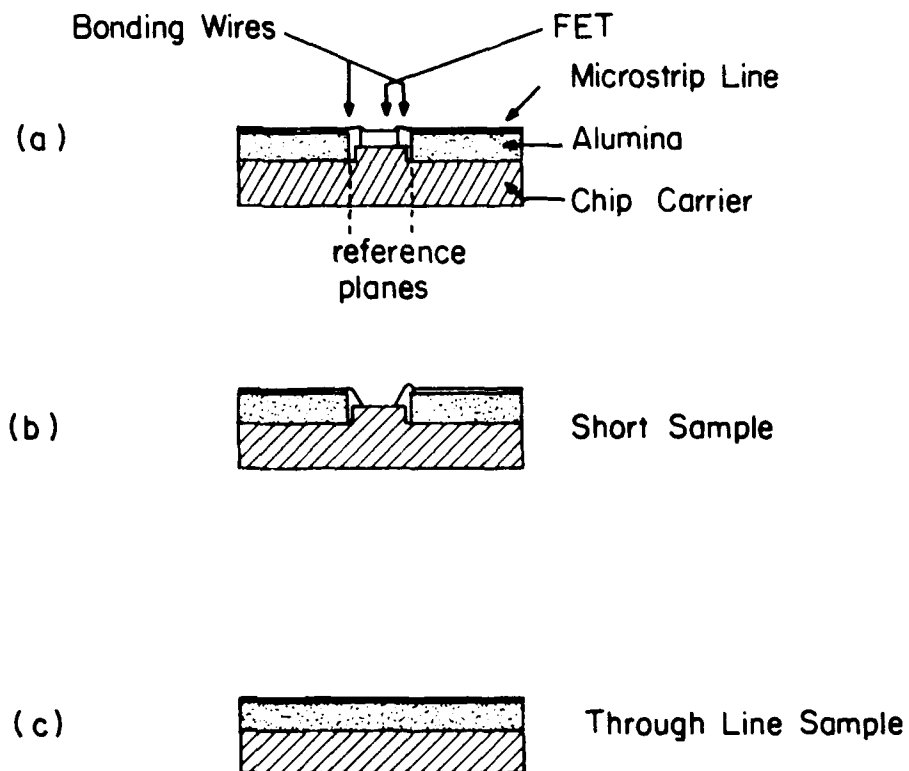


Figure 30. Chip carrier (a) and short (b) and through line (c) samples.

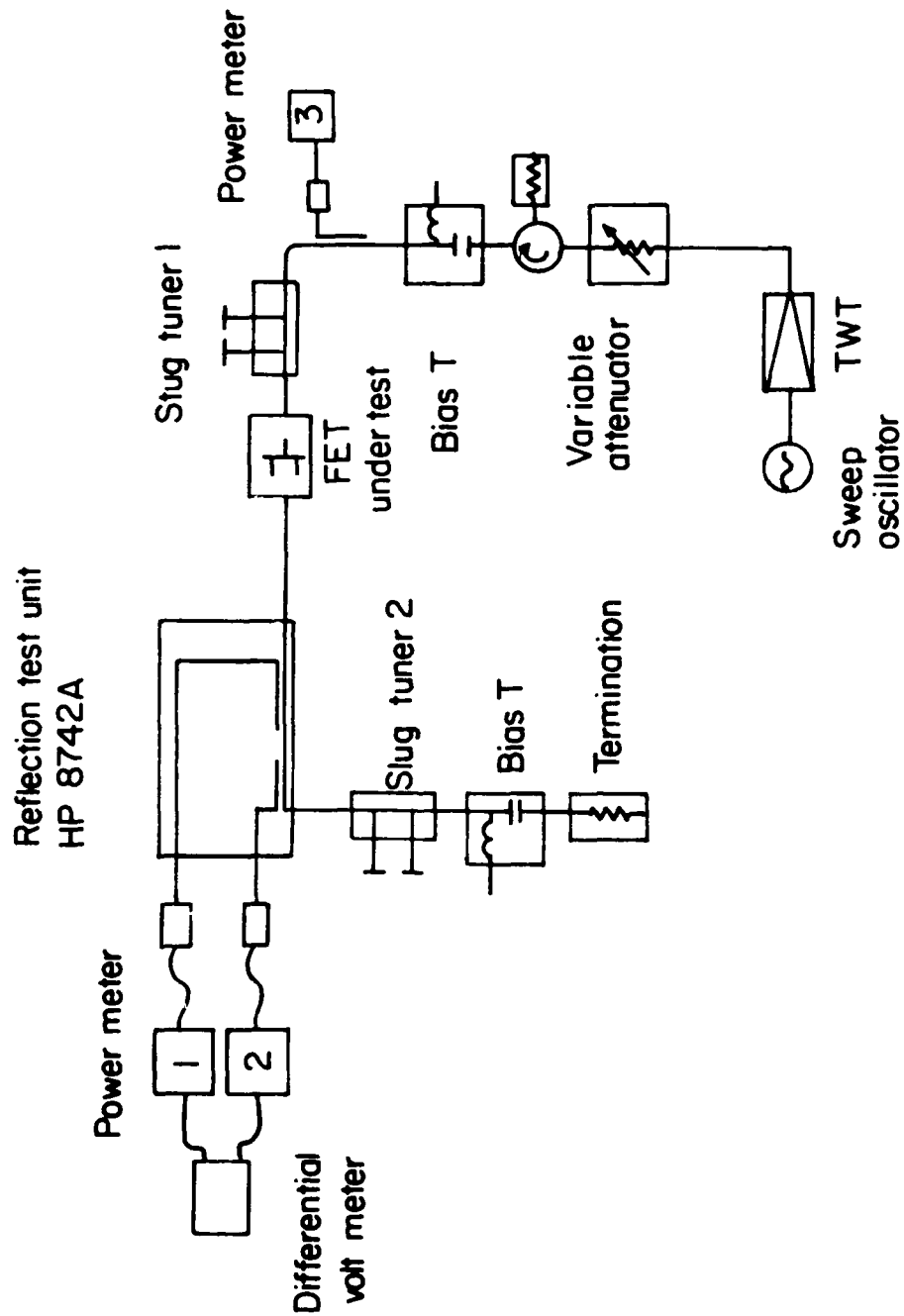


Figure 31. Power measurement set-up.

PBN-80-1002

NAME	TITLE	DWG NO
SMITH CHART FORM 8285PR (2-48)	KAY ELECTRIC COMPANY, PINE BROOK, N.J. 07449 PRINTED IN U.S.A.	DATE

IMPEDANCE OR ADMITTANCE COORDINATES

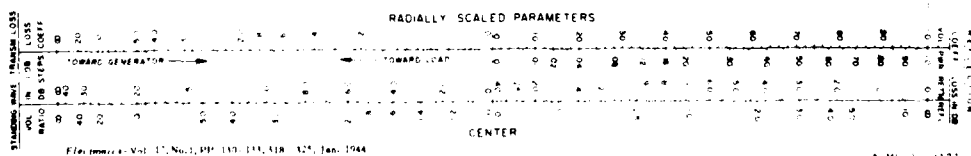
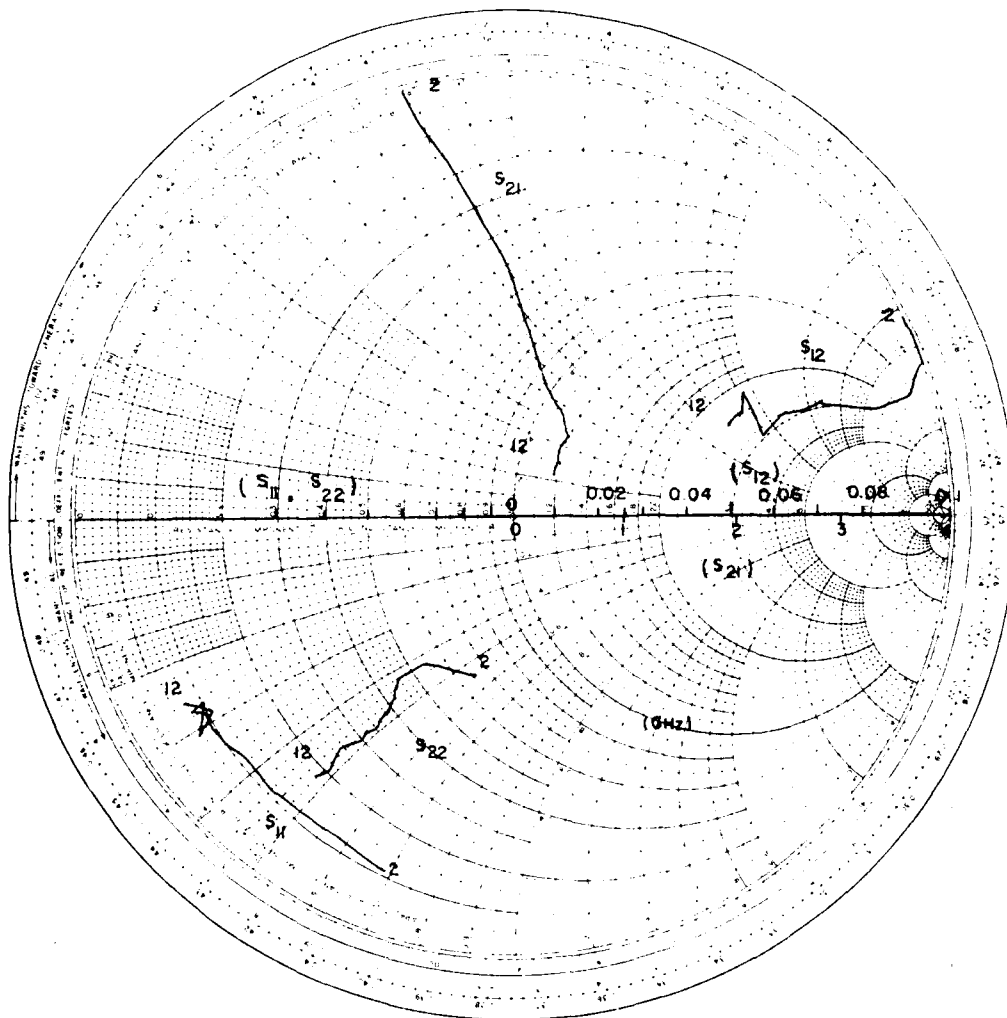


Figure 32. S-parameters for a device from wafer 7B-218A.

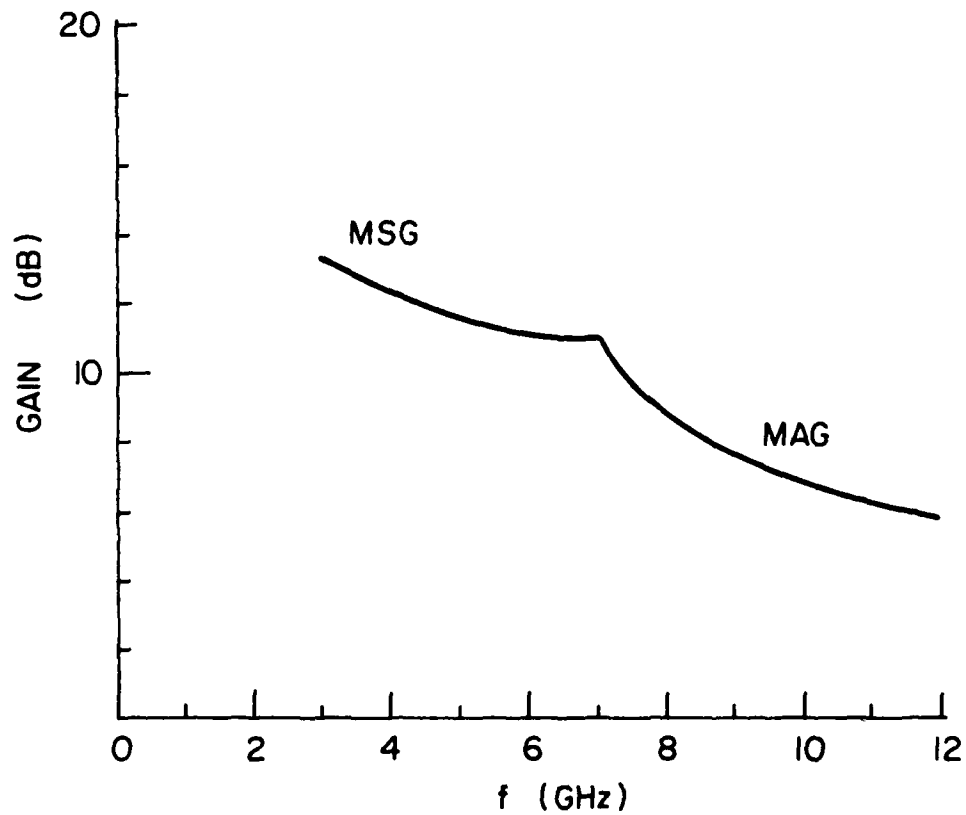


Figure 33. Maximum stable gain (MSG) and maximum available gain (MAG) for a device from wafer 7B-218A.

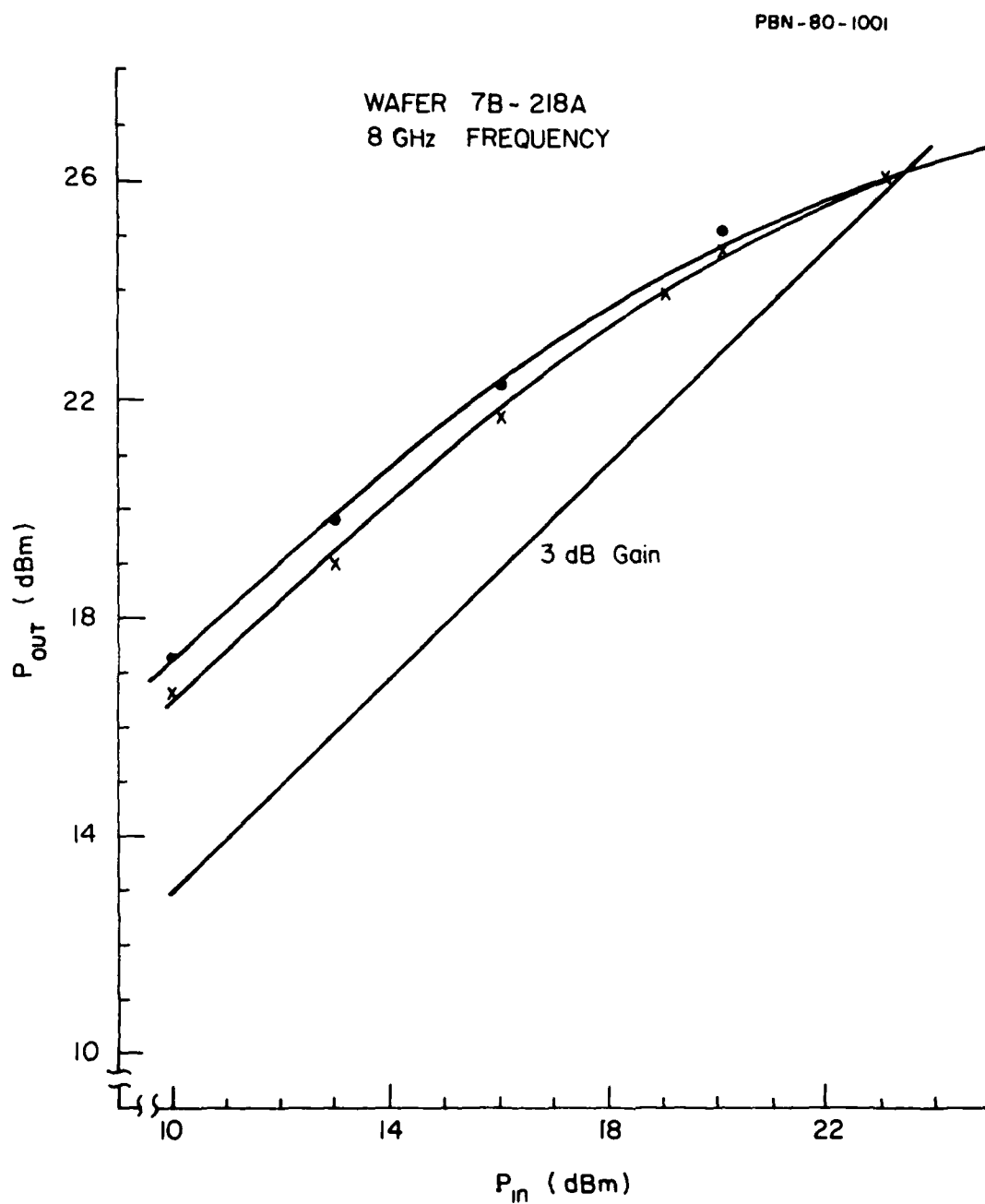


Figure 34. Input versus output power characteristics for a device from wafer 7B-218A. 8.8 volts drain bias, -0.5 volts gate bias; X 7.5 volts drain bias, -0.1 volts gate bias.

Drain biases of 8, 10, and 12 V were tried at 8 to 10 GHz with the gate voltage tuned between 0.5 and 2 V for maximum power, usually resulting in about 200 mA drain current. Power characteristics for this device are shown in Fig. 35, which shows 1.2 W at 0 dB gain and 1.0 W at 3 dB gain at 8 GHz with a 12 V drain bias. G_{\max} was calculated to be 6.5 dB at 8 GHz with a rolloff of about 8 dB per octave.

In general the electrical performance of devices from these two wafers did not differ significantly from similar devices with alloyed contacts. Devices from both wafers were delivered to the Office of Naval Research for evaluation of their reliability under prolonged operation.

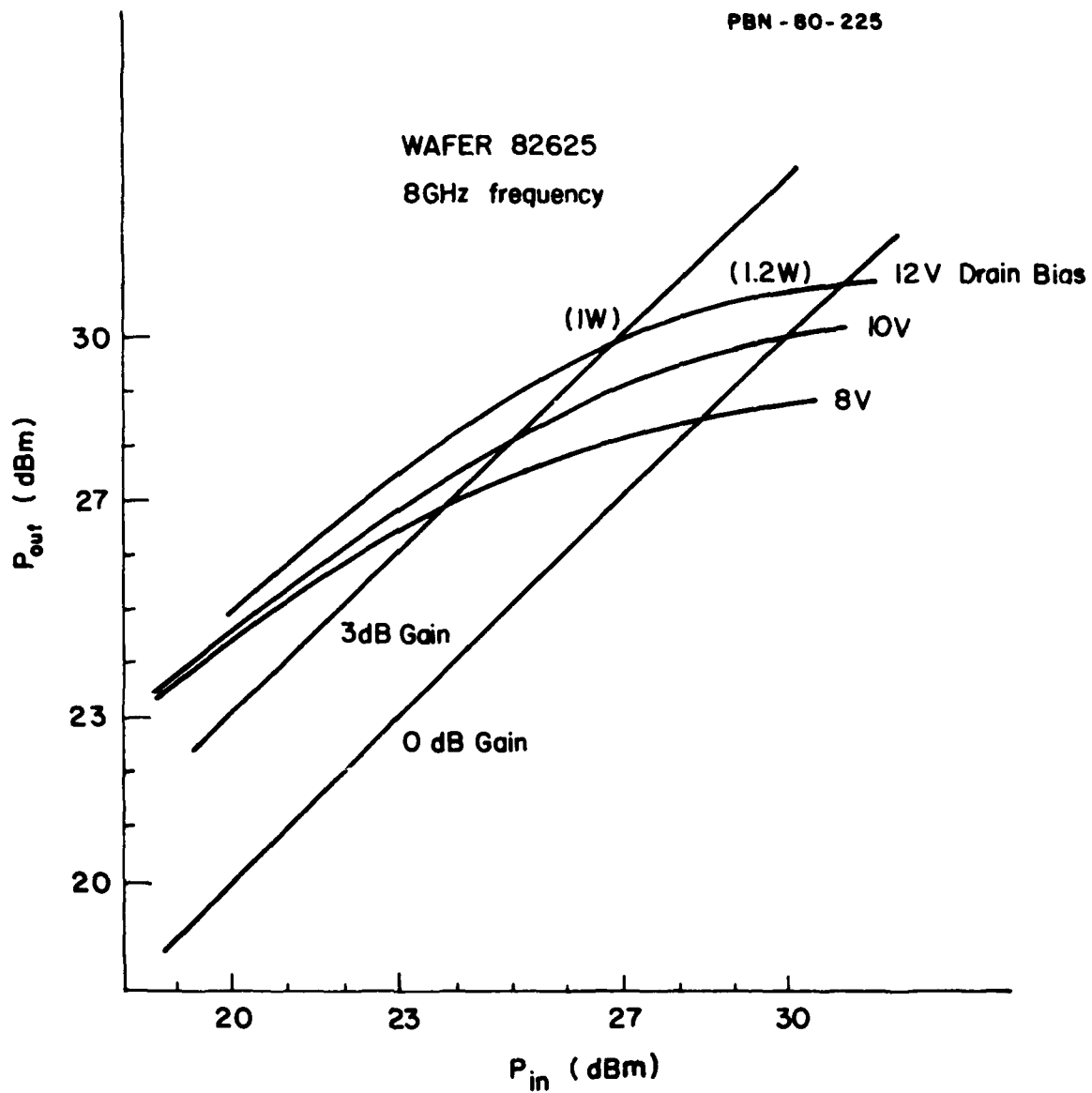


Figure 35. Power FET output power versus input power, wafer 82625, device #2.

SECTION VI

SUMMARY

Unalloyed, refractory-metal, ohmic contacts were formed on n-type GaAs by preparing surfaces having over 10^{19} carriers/cm³ prior to metal deposition. Such highly doped n⁺⁺ layers were made in two ways. One procedure was to adjust conditions during the final stage of vapor phase epilayer growth to favor an increased concentration of silicon donors on gallium lattice sites. Shallow layers doped at or above 10^{19} /cm³ were formed and high-performance power FETs with unalloyed TiPtAu contacts were made. The specific contact resistivity varied between 8×10^{-6} and 9×10^{-5} ohm cm² from sample to sample. By comparison, alloyed NiAuGe contacts on these layers were typically 1.2×10^{-6} ohm cm² and the thermal stability in terms of the percentage increase in resistivity after anneals at 250°C was about the same for alloyed and unalloyed contacts. However, the gate leakage under reverse bias was remarkably low on some of the devices with unalloyed contacts, suggesting that there may be an indirect benefit for power FETs which outweighs the higher contact resistance. Furthermore, it is quite possible that the surface layer concentration and thickness can be increased to yield higher reproducibility and lower resistivity. For our samples the concentration was about 10^{19} /cm³ to a depth of about 100 Å, values which are only marginally adequate for ohmic contacts.

The second approach, radiation-annealed selenium implants, began auspiciously when implants and pulse electron beam exposures covering an entire surface yielded layers about 2000 Å thick having well over 10^{19} carriers/cm³ and up to 8×10^{19} carriers/cm³. Contact resistivities were as low as 3×10^{-7} ohm cm² and thermal stress tests at 250°C for as long as 8½ hours had little effect except to reduce resistivities which were initially above 10^{-6} ohm cm². These reductions occurred in spite of a concurrent 50 percent increase in the sheet resistance of unmetallized areas.

Use of these superlative contacts in a power FET configuration was unsuccessful because unimplanted channel regions suffered severe reduction in carrier concentration during anneal and attempts to selectively mask channels from incident electrons resulted in high thermal gradients and topographic irregularities

at the perimeters of openings in the mask. Hence the advantage of PEBA over pulsed laser annealing with regard to surface smoothness was partially lost in this mode of exposure.

Attempts to select PEBA fluences within a narrow band which might yield sufficiently highly doped contact layers without destroying channel-type regions and without selective masking was more promising but still unsuccessful. SEM photos of these samples had interesting features suggestive of melting in implanted areas but not elsewhere. Once again distortions appeared, this time at boundaries between implanted and unimplanted areas. Judicious selection of anneal parameters could possibly give suitable conditions for device applications. For example, lateral thermal gradients at the GaAs surface would be reduced by using a layered encapsulant having thicknesses over channel and contact regions adjusted to vary the energy deposited in the respective regions in a gradual rather than discontinuous way. The laser approach would offer more flexibility in this regard. Although the first order effect of either electron or light under similar levels of absorbed power is to produce rapid heating followed by a rapid quench, the energy transfer mechanisms are more complex and variable for light and therefore it would be more amenable to control of the temporal and spatial details of energy deposition through choice of mask and exposure parameters. Large-area laser beams would reduce the objectionable surface irregularities characteristic of the raster scan of discreet pulses used for our trial laser exposures.

The potential excellence of radiation-annealed contacts justifies continued efforts to find ways to form them without introducing the deleterious side effects described in this report. These efforts would benefit from a better understanding of the changes induced in GaAs by pulse annealing and how these changes depend on such variables as ion implant and anneal conditions, the properties of protective surface films and the presence of discontinuities such as boundaries between implanted and unimplanted regions and masked and unmasked areas.

REFERENCES

1. W. B. Edwards, W. A. Hartman and A. B. Torrena, Solid-State Electron. 15, 387 (1972)
2. D. A. Abbott and J. A. Turner, IEEE Trans. Microwave Theory Tech. MTT-24, 317 (1976)
3. T. Irie, I. Nagasako, H. Kohzu and K. Sikido, IEEE Trans. Microwave Theory Tech. MTT-24, 322 (1976)
4. A. M. Andrews and N. Holonyak, Solid-State Electron. 15, 601 (1972)
5. G. Y. Robinson, Solid-State Electron. 18, 331 (1975)
6. M. Wittmer, R. Pretorios, J. W. Mayer and M. A. Nicolet, Solid-State Electron. 20, 433 (1977)
7. M. N. Yoder, Solid-State Electron. 23, 117 (1980)
8. C. Y. Chang, Y. K. Fang and S. M. Sze, Solid-State Electron. 14, 541 (1971)
9. R. S. Popović, Solid-State Electron. 21, 1133 (1978)
10. A. K. Sinha, T. E. Smith, M. H. Read and J. M. Poate, Solid-State Electron. 19, 489 (1976)
11. R. S. Pounds, M. A. Saifi and W. C. Hahn, Jr., Solid-State Electron. 17, 245 (1974)
12. S. Margalit, D. Fekete, D. M. Pepper, C. Lee and A. Yariv, Appl. Phys. Lett. 33, 346 (1978)
13. G. Eckhardt, C. L. Anderson, L. D. Hess and C. F. Krumm, Laser-Solid Interactions and Laser Processing - 1978, Ed. S. D. Ferris, H. J. Leamy and J. M. Poate (New York: American Institute of Physics, 1979), p. 641
14. R. B. Gold, R. A. Powell and J. F. Gibbons, Laser-Solid Interactions and Laser Processing - 1978, Ed. S. D. Ferris, H. J. Leamy and J. M. Poate (New York: American Institute of Physics, 1979) p. 635
15. P. A. Barnes, H. J. Leamy, J. M. Poate, S. D. Ferris, J. S. Williams and G. K. Celler, Appl. Phys. Lett. 33, 965 (1978)
16. S. G. Liu, C. P. Wu and C. W. Magee, Laser and Electron Beam Processing of Materials, Materials Research Society Symposium Abstracts, Cambridge, Massachusetts, November 27-30, 1979, p. 69

17. H. B. Harrison and J. S. Williams, Laser and Electron Beam Processing of Materials, Materials Research Society Symposium Abstracts, Cambridge, Massachusetts, November 27-30, 1979, p. 123
18. B. O. Seraphin and H. E. Bennett, Semiconductors and Semimetals, Vol. 3, Ed. R. K. Willardson and A. C. Beer (New York: Academic Press, 1967)
19. A. C. Greenwald, A. R. Kirkpatrick, R. G. Little and J. A. Minnucci, J. Appl. Phys. 50, 783 (1979)
20. P. A. Pianetta, C. A. Stolte, and J. L. Hansen, Appl. Phys. Lett. 36, 597 (1980)
21. P. A. Barnes and A. Y. Cho, Appl. Phys. Lett. 33, 651 (1978)
22. P. L. Howe, W. W. Hooper, B. R. Cairns, R. D. Fairman and D. A. Tremere, Semiconductors and Semimetals, Vol. 7A, Ed. R. K. Willardson and A. C. Beer (New York: Academic Press, 1971), p. 178
23. H. H. Berger, J. Electrochem. Soc. 119, 507 (1972)
24. R. L. Mozzi, W. Fabian and F. J. Piekarski, Appl. Phys. Lett. 35, 337 (1979)
25. J. F. Gibbons, W. S. Johnson and S. W. Mylroie, Projected Range Statistics, 2nd Edition (Stroudsburg, Penn: Dowden, Hutchinson & Ross, Inc., 1975).
26. P. L. Hower and N. B. Baechtel, "Current Saturation and Small-Signal Characteristics of GaAs FET Transistors," IEEE Trans. on ED, volume ED-20 No. 3, March 1973, pp. 213-220.

9/80

DISTRIBUTION LIST - TECHNICAL REPORTS
CONTRACT N00014-78-C-0622

Code 427	4	Dr. H. C. Nathanson	1
Office of Naval Research		Westinghouse Research and	
Arlington, VA 22217		Development Center	
Naval Research Laboratory		Beulah Road	
4555 Overlook Avenue, S.W.		Pittsburgh, PA 15235	
Washington, D.C. 20375		Dr. Daniel Chen	1
Code 6811	1	Rockwell International	
6850	1	Science Center	
6815	1	P.O. Box 1085	
		Thousand Oaks, CA 91360	
Defense Documentation Center	12	Dr. C. Krumn	1
Building 5, Cameron Station		Hughes Research Laboratory	
Alexandria, VA 22314		3011 Malibu Canyon Road	
Dr. Y. S. Park	1	Malibu, CA 90265	
AFWAL/DHR		Mr. Lothar Wandinger	1
Building 450		ECOM/AMSEL/TL/IJ	
Wright-Patterson AFB		Fort Monmouth, NJ 07003	
Ohio 45433		Dr. Harry Wieder	1
ERADCOM	1	Naval Ocean Systems Center	
DELET-M		Code 922	
Fort Monmouth, NJ 07703		271 Catalina Blvd.	
Texas Instruments	1	San Diego, CA 92152	
Central Research Lab		Dr. William Lindley	1
M.S. 134		MIT	
13500 North Central Expressway		Lincoln Laboratory	
Dallas, TX 75265		F124 A, P.O. Box 73	
Attn: Dr. W. Wisseman		Lexington, MA 02173	
Dr. R. M. Malbon/M.S. 1C	1	Commander	1
Avantek, Inc.		U.S. Army Electronics Command	
3175 Bowers Avenue		V. Gelinovatch	
Santa Clara, CA 94304		(DRSEL-TL-IC)	
Mr. R. Bierig	1	Fort Monmouth, NJ 07703	
Raytheon Company		RCA	1
28 Seyon Street		Microwave Technology Center	
Waltham, MA 02154		Dr. F. Sterzer	
Dr. R. Bell, K-101	1	Princeton, NJ 08540	
Varian Associates, Inc.			
611 Hansen Way			
Palo Alto, CA 94304			

Hewlett-Packard Corporation
Dr. Robert Archer
1501 Page Mill Road
Palo Alto, CA 94306

1

D. Claxton
MS/1414
TRW Systems
One Space Park
Redondo Beach, CA 90278

1

Watkins-Johnson Company
E. J. Crescenzi, Jr./
K. Niclas
3333 Hillview Avenue
Stanford Industrial Park
Palo Alto, CA 94304

1

Professor L. Eastman
Phillips Hall
Cornell University
Ithaca, NY 14853

1

Commandant
Marine Corps
Scientific Advisor (Code AX)
Washington, D.C. 20380

1

AIL TECH
612 N. Mary Avenue
Sunnyvale, CA 94086
Attn: G. D. Vendelin

1

Communications Transistor Corp.
Dr. W. Weisenberger
301 Industrial Way
San Carlos, CA 94070

1

Professors Hauser and
Littlejohn
Department of Electrical
Engineering
North Carolina State University
Raleigh, NC 27607

1

Microwave Associates
Northwest Industrial Park
Drs. F. A. Brand/J. Saloom
Burlington, MA 01803

1

Professor J. Beyer
University of Wisconsin-Madison
750 University Avenue
Madison, WI 53706

1

Commander, AFAL
AFWAL/AADM
Dr. Don Rees
Wright-Patterson AFB, Ohio 45433

1

W. Perkins
General Electric Company
Electronics Lab 3-115/B4
P. O. Box 4840
Syracuse, NY 13221

1

Professor Walter Ku
Phillips Hall
Cornell University
Ithaca, NY 14853

1

Professor Rosenbaum and
Wolfe
Washington University
Semiconductor Research Laboratory
P. O. Box 1127
St. Louis, Missouri 63130

1

Commander
Harry Diamond Laboratories
Mr. Horst W. A. Gerlach
2800 Powder Mill Road
Adelphia, MD 20783

1

Advisory Group on Electron
Devices
201 Varick Street, 9th floor
New York, NY 10014

1

